FACHHOCHSCHULE AACHEN
ABTEILUNG JÜLICH

Diplomarbeit

Jürgen Broders

SPUTTERN VON SUPRALEITENDEN DÜNNEN FILMEN FÜR RADIOFREQUENZ BESCHLEUIGUNGSRESONATOREN

Erste Ergebnisse der Anwendung der Sputtertechnologie für Resonatoren des TESLA-types

Referent FH Aachen: Prof. Dr. M. Müller-Veggian

Co-Referent INFN-LNL: Dr. V. Palmieri

Diese Arbeit wurde durchgeführt am
Istituto Nazionale di Fisica Nucleare
Laboratori Nazionali di Legnaro

INFN

Legnaro. Juli 1995

Acknowledgements

This work has been a first step for a scientific collaboration on Superconducting Cavities between Fachhochschule Aachen and INFN Laboratori Nazionali di Legnaro. It was made under a Erasmus fellowship.

The work was part of the CERN - INFN Collaboration on Superconducting Cavities.

I would like to thank my supervisors, Prof. Dr. M. Müller-Veggian at FH Jülich and Dr. V. Palmieri for their support during my work.

Sincerest thanks are due to Dr. Vladimir Ruzinov for introducing me in most of the experimental techniques, for many interesting discussions and for his excellent support throughout the project.

I also wish to thank Dr. Sergej Stark for the rf measurements, Dr. Illya Kulik for useful discussions about cryogenics, Fabrizio Stivanello for the chemical treatments of the cavities and Renato Preciso for a lot of technical assistance. Furthermore I am deeply indebted to thank Jörg Kaiser and Marco Pilati for their assistance and for their splendid friendship.

Einleitung

Unter den Hochenergiephysikern herscht eine weitreichende Übereinstimmung, daß ein Elektron-Positron-Collider mit einer Mittelpunktenergie von 500 Gev und einer Luminosität über $10^{33}cm^{-2}s^{-1}$ als möglicher, zukünftiger Beschleuniger nach dem Large Hadron Collider (LHC) in Betracht gezogen werden sollte.

Mit dem erfolgreichen Betrieb von supraleitenden Hoch-Frequenz Strukturen in den Beschleunigern TRISTAN (KEK), LEP (CERN) und HERA (DESY), ist die Bedeutung der Supra-leitung für Hochenergie - Elektronen - Beschleuniger gewachsen.

Wenn noch höhere Gradienten erreicht werden können und die Kosten weiter sinken, gibt es Gründe, die dafür sprechen einen vollständig supraleitenden TeV Linear-Collider zu entwickeln. Bereits jetzt arbeiten Wissenschaftler aus aller Welt am Design eines derartigen Collider

Unter diesen Plänen ist nur einer, der sowohl supraleitende Beschleunigungsstrukturen, als auch niedrige Frequenzen aufweist, nämlich der sogenante TeV Energy Superconducting Linear Collider (TESLA). In diesem Rahmen plant die TESLA R&D Gruppe bis 1997 einen Prototyp, wie die TESLA Test Facility (TTF) in Betrieb zu haben und ausgereifte Pläne für den zukünftigen Linear Collider zu entwickeln. Mit den Erfahrungen von Bau und Betrieb dieser Testanlage wird es möglich sein, die unterschiedlichen Vorschläge zu vergleichen, um die beste Technik auszuwählen.

Hauptkriterien in dieser Auswahl werden die technischen Eigenschaften, Minimierung der technische Risiken und das mögliche Optimierungspotential sein. Dabei sind nicht zuletzt die Betriebskosten von entscheidender Bedeutung

Von höchstem Interesse ist es auch, zu beweisen, daß Beschleunigungsgradienten von 15MV/m oder mehr, zuverlässig zu erreichen sind und daß das Potential für Gradienten von 25MV/m in 9-Zelligen Resonatoren da ist.

Niob beschichtete Kupfer-Resonatoren sind eine vielversprechende Alternative zu den herkömmlichen massiven Niob-Resonatoren, besonders wenn man die Zahl von 20000 Stück berücksichtigt. Die Verbindung der supraleitenden Eigenschaften einer dünnen Niobschicht mit der guten Wärmeleitfähigkeit von Kupfer bietet bessere Hochfrequenzeigenschaften und darüberhinaus geringere Materialkosten. Aber der wirkliche Durchbruch der Sputtertechnologie liegt in dem großen Potential. Neue Horizonte können mit dieser Technik eröffnet werden: Materialien mit höheren kritischen Temperaturen, Beschichtungen gegen Feldemission über der Niobschicht und Unterschichten als Barrieren gegen die Diffusion von Verunreinigungen aus dem Substrat können als Möglichkeiten genannt werden.

Andere Konstruktionsmaterialien als Kupfer sind momentan technisch noch nicht realisierbar, aber es ist klar daß Hohlraumresonatoren der nächsten Generation neue Ideen und innovative Fabrikationstechniken erfordern.

Im folgenden ist das Magnetron Sputtering System beschrieben, das für das Sputtern von Kupfer-Monocell-Resonatoren des TESLA-types konstruiert und gebaut wurde.

Weil zu Beginn dieser Arbeit noch nicht entschieden war, welche Frequenz für TESLA gewählt werden würde, ist die Arbeit mit 1.5 GHz Cavities gestartet worden. Sobald die Forschung mit 1.5 Ghz Resonatoren gute Ergebnisse liefert, ist der Wechsel auf 1.3 GHz kein großes Problem.

Für zukünftige Forschungsarbeiten in Hinblick auf die mögliche Verwendung von Niob gesputterten Resonatoren ist diese Arbeit ein erster Schritt.

PREFAZIONE

E' convinzione diffusa nella comunita' della Fisica delle alte enmergie, che un collider elettrone-positrone ad energie di centro di massa di 500 Gev e luminosita' superiore a $10^{33}cm^{-2}sec^{-1}$ sia la macchina acceleratrice piu' probabile dopo LHC.

Il successo di operazioni come la messa in opera di strutture superconduttrici in Radiofrequenza del tipo TRISTAN a KEK, LEP al CERN, HERA a DESY., ha contribuito a far levitare l' importanza dell' applicazione della Superconduttivita' agli acceleratori di particelle. Se il numero di MV/m ottenibili in cavita' continueranno ad aumentare e si riuscira' ad abbattere i costi, diventera' assolutamente realistico pensare ad un collider lineare interamente superconduttivo che arrivi ad energie del TeV. In giro per il mondo esiste un certo numero di collaborazioni che spingono per collider lineari. Fra questi pero' TESLA e' l'unico disegno di macchina che preveda superconduttivita' e basse frequenze di risonanza delle cavita'. In tale contesto la collaborazione TESLA prevede la messa a punto di un banco di test, dal nome TTF, in cui sara' possibile mettere alla prova le tecnologie piu' promettenti.

La chiave di volta per la costruzione di TESLA sara' l' esperienza fatta su TTF. Le tecnologie di fabbricazione dei risonatori dovranno essere affidabili, a basso rischio ed a basso costo. L' obbiettivo consiste nell' ottenimento in cavita' a nove celle a 1.3 GHz di gradienti acceleranti di 15 MV/m in una prima fase e 25 MV/m in un secondo momento.

In tal contesto le cavita' in Rame ricoperte per sputtering di Niobio rappresentano una valida alternativa alla tecnologia tradizionale del Niobio massiccio, soprattutto quando ci si confronta con un numero di pezzi dell' ordine di 20.000. Interfacciare le proprieta' superconduttive di un sottile strato di Niobio con quelle di stabilita' termica del Rame, offre prestazioni potenzialmente migliori accompagnate da un costo piu' basso. Ma il grosso vantaggio della tecnologia dello sputtering e' racchiuso nelle potenzialita' offerte dalla tecnica: nuovi materiali a temperatura critica piu' elevata, ricoprimenti protettivi contro l'emissione di campo, barriere di diffusione fra il substrato ed il film, nuovi materiali per il substrato. Tutte queste cose

sono al momento ancora lontane dall' applicabilita'. ma e' chiaro che diventeranno la parola chiave per la costruzione di cavita' di nuova generazione.

Index

1. Introduction

1.1 Preface

Within the high-energy physics community there is a widespread consensus, that an electron-positron collider with a center of mass energy of 500 GeV and luminosity above 10^{33} $cm^{-2}sec^{-1}$ should be considered as a possibility for the next accelerator facility after the Large Hadron Collider (LHC).

With successful operation of Superconducting Radio-Frequency structures in TRISTAN at KEK, LEP at CERN, HERA at DESY, the importance of applying superconductivity to high electron accelerators is growing rapidly. If gradients continue to improve and costs drop, there will be many compelling attractions to a fully superconducting TeV linear collider. Worldwide, there is a number of groups pursuing linear collider design efforts. Among them the only machine design pursuing for both superconducting accelerating structures and low frequency is the one of the TeV Energy Superconducting Linear Collider (TESLA).[1] In such a framework the TESLA R&D group plans to have working prototype test facilities as the TESLA Test Facility (TTF), and well-developed collider designs in the 1997 time scale. After experience with implementation and operation of the TTF it will be possible to start making relative evaluations of the different proposals, looking forward to the selection of the most promising technology.

Key in this selection will be technical merit, minimisation of technical risk, and potential for optimisation of performance. Equally important, however will be operating costs.

Of highest interest is to prove the feasibility of reliably achieving accelerating gradients of 15 MV/m or more, and the clear potential to gradients of 25 MV/m in 1.3 GHz nine-cell resonators.

Niobium sputter-coated Copper cavities are a promising alternative to the traditional bulk cavities, especially when dialling with numbers of pieces of the order of 20.000. The interface of the superconductive properties of a thin layer of Niobium with the heat exchange bulk properties of Copper, provide potentially higher rf performances together with a saving in material cost. But the real breakthrough of the sputtering

technique is disclosed in its potentialities: new horizons could be opened by the sputtering technique. New materials with critical temperatures higher than the one of Niobium, over-layers against field emission, under-layers as diffusion barriers from the substrate, new materials instead than Copper are at the moment to far from application, but it is clear that cavities of a new generation require new ideas and powerful fabrication techniques.

In the following it is described the magnetron sputtering configuration designed and built for Niobium sputtering Copper monocell resonators of TESLA-type. The work is performed onto 1.5 GHz cavities, since the research at Legnaro National Laboratories (LNL) started when the frequency choice for TESLA was not yet clear; moreover as soon as the research on 1.5 GHz will provide results, the change from 1.5 GHz to 1.3 GHz will be a minor problem.

For future development in search for the feasibility of Niobium sputtered cavities this work is only a preliminar operation.

1.2 Radiofrequency Resonators

Each accelerator consists of rf accelerating structures and magnets to guide and focus the particle beam. The accelerating structures are composed of resonating cavities, which are energy storage devices employed for the radiofrequency and microwave range. The working principle is equivalent to a classical RLC resonant circuit.[2] The electromagnetic energy oscillates back and forth from entirely electric to entirely magnetic form of energy. The RLC circuit will resonate at a frequency $\omega_0 = 1/\sqrt{LC}$. To make the circuit resonating at higher frequencies, a possibility is to decrease L as much as possible.

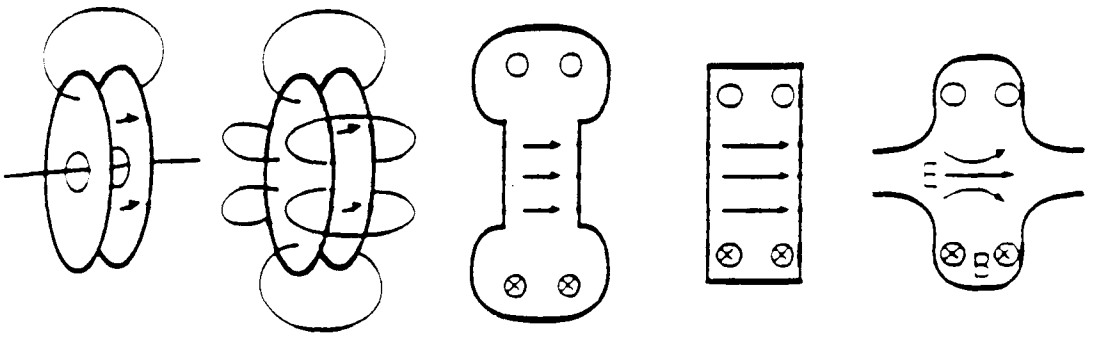

Fig. 1-1 Transformation of a L-C circuit into an accelerating cavity [3]

Inside the cavities different resonances can be excited, as shown in Fig. 1-1, for accelerating cavities usually the TM_{010} mode is chosen. This mode has a longitudinal electric field along the cavity axis, which is surrounded by the circular field lines of the magnetic field. For highly relativistic particles such as electrons and positrons several cavity cells can be mounted in series. Each cell in this system must be coupled with the following.

The favourite coupling mode of accelerating structures is the so called π-mode, represented in fig. 1-2 and 1-3 .

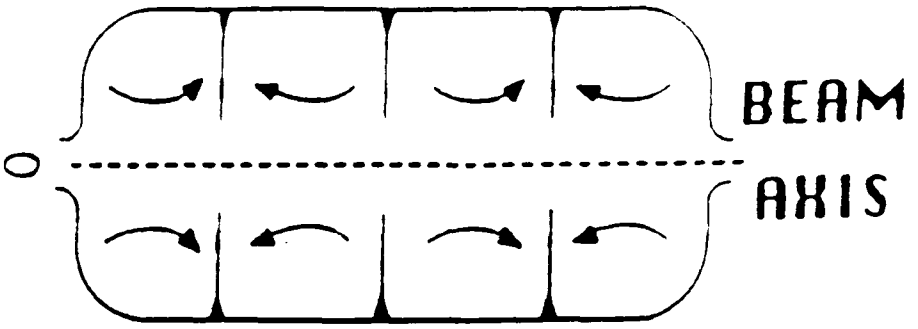

Fig. 1-2 *A multi-cell cavity excited in the Π-mode. This mode is characterised by the fact that the accelerating fields in each pair of cavities are equal in magnitude and opposite in direction*

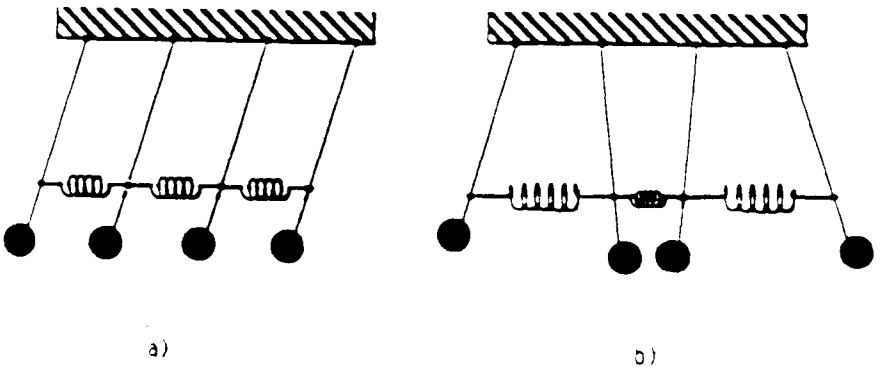

Fig. 1-3 *The coupled pendula analogue* [3]
a) The zero mode: The phase difference is zero
b) The Π-mode: The phase difference is Π

If the velocity of the particle bunch is synchronised with frequency and phase of the rf fields in the cavity the bunch will be accelerated in each cell: In the first cell the field is parallel to the bunch, in the second cell it is antiparallel, but it becomes parallel one semi-cycle later just when the beam arrives. To be accelerated in every cycle the particles velocity has to be adjusted to the effective electric length $v=b\cdot c$ and to the resonant frequency f_0. This leads to the condition

$$\omega_0 \cdot d \leq \pi \cdot b \cdot c \qquad (1.1)$$

That means that resonant frequencies for electron cavities (b~1) range between 350 and 3000 MHz since d has values generally between 5 and 10 cm.

Independently of which resonance is excited inside the cavity, the field oscillation will get damped, if the cavity is left in free oscillation. This is caused to the non perfect conductivity of the resonator walls and to the losses through resonator ports, if present.
So the energy initially stored into the cavity will exponentially decay with a damping time proportional to the quality factor Q_0.

$$W(t)=W_0 \cdot e^{-(W_0 Q_0 t)} \tag{1.2}$$

The quality factor can be defined as

$$Q_0=\omega_0 \cdot W/P_d \tag{1.3}$$

where W is the energy stored in the cavity, P_d the dissipated power and ω_0 the resonant frequency.[4] Since the energy leakage and also the frequency selectivity is proportional to the quality factor the ultimate Q is desired.
The quantity of highest interest for particle physicists of course is the accelerating field that can obtained in a cavity. Higher accelerating fields allows a greater acceleration, i.e. a higher particle energy within a given structure length. Vice versa high fields allows to build accelerating structures of shorter length, which results in much lower costs.

The TESLA collaboration has chosen a nine cell cavity with a resonance frequency of 1300 MHz. A Q_0 better than $5 \cdot 10^9$ at a accelerating field of 25 MV/m is required.[1]

1.3 Fundamentals of Superconductivity

Three years after the first liquefaction of helium in 1911, Heike Kammerlingh-Onnes[5] discovered that mercury completely lose its resistivity at temperatures below 4.15K. Today many other metals and compounds are known as superconductors. Measurements of the decay time of a current into a superconducting ring[6] proof that the resistivity of a superconductor is below 10^{-27} Ωcm. So one can indeed speak of a total vanishing of electrical resistance.

The abrupt vanishing of resistance at a certain temperature in super-conductors is a phase transition in another state. The temperature Ts in which this phenomenon occurs is the critical temperature Tc. The pure element with the highest transition temperature is niobium (9.26K).and for many years the highest Tc in a compound was also a Niobium-based one (Nb_3Ge. T_C=23.2K). The discovery of a new class of superconducting materials by Bednorz and Mueller[7] make it possible to find a compound with a Tc higher than liquid nitrogen temperature.

Compound	T_c (K)	Compound	T_c (K)
Nb_3Sn	18.05	$Pb_{0.7}Bi_{0.3}$	8.45
Nb_3Ge	22.3	V_3Si	17.1
NbN	16	$(SN)_x$	0.26
NbO	1.2	$(BEDT)_2Cu(NCS)_2$	10
$BaPb_{0.75}Bi_{0.25}O_3$	11	$La_{1.8}Sr_{0.2}CuO_4$	38
UBe_{13}	0.75	$Bi_2CaSr_2Cu_2O_{8+x}$	90

Table 1.1: Critical temperatures of some elements and compounnds [8]

The absence of any resistance is the well-knownst property of superconductors. but there are also some other remarkable characteristics. In 1933. Meissner and Ochsenfeld[9] found that magnetic fields is squeezed out of a superconductor at temperatures below Tc. In normal materials there appears a finite induction B given by B=μH. when a magnetic field is applied. In diamagnetics (μ<1), the applied field is weakened and the induction B becomes smaller than H. In superconductors the magnetic

permeability is zero, corresponding to ideal diamagnetism. This effect arise due to an electric current induced in a thin surface layer, in which the magnetic field penetrates. The magnetic field of the electric current oppose the applied field: the result is zero magnetic induction inside the sample. The field penetration depth is one of the main characteristics of a superconductor. Its thickness is usually in the range of a few hundreds Angstroms. If the magnetic field increases at some certain values, called the critical field, it destroys superconductivity and the sample goes in the normal state. At zero temperature the critical field has a maximum, at T=Tc the critical field is zero. Such a behaviour can approximately given by the formula

$$H_C(T) = H_{\infty} (1-T/Tc)^2 \qquad (1.4)$$

where Hco is the value of the critical field at zero temperature. Depending on the particular superconductor, the critical field can assume values in a rather wide range, but its existence is an universal feature for all superconducting materials.

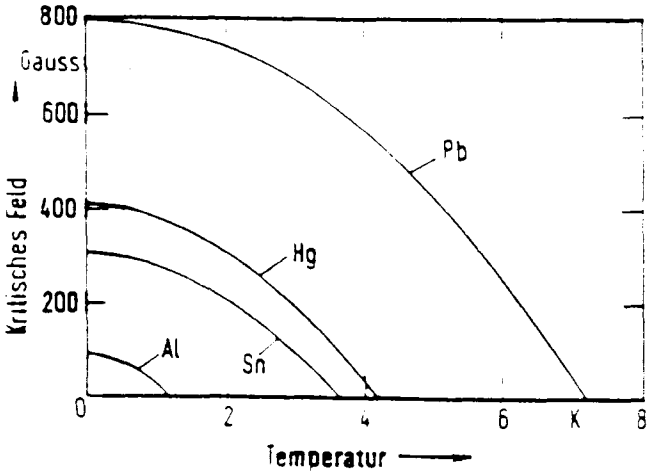

Fig. 1-4 Critical field versus temperature of some elements [10]

From these figure one can see, that the critical fields are rather low and not sufficient for technical applications. The presented superconductors are "Type I superconductors". These type shows a sharp transition from the superconducting to the normal state for values less than Tc. Higher critical fields provide "Type II superconductors". These class of superconductors are different in regard to their magnetic behaviour. In contrary to Type I superconductors they have two critical fields: H_{C1}, below which the material is entirely superconducting and an upper critical field H_{C2}, over which the sample is completely normal conducting. Between these two fields, the magnetic flux penetrates partially in the material, which is divided in normal conducting filaments surrounded by superconducting regions. Niobium and all other materials of interesting for TESLA type cavities are superconductors of the second type.

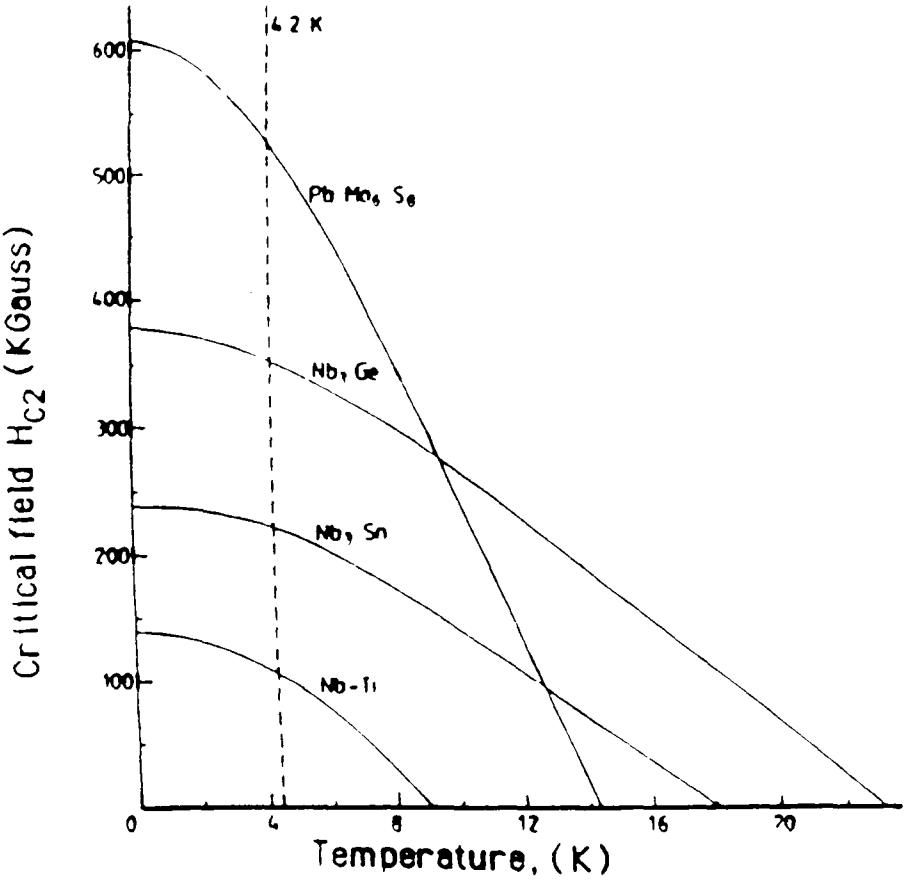

Fig. 1-5 *Critical fields of some type II compounds*

Microscopic theory

A systematic theory of superconductivity, which explained the nature of this phenomenon, was formulated in 1957 by Bardeen, Cooper and Schrieffer.[11] It based on a "condensation" of electrons into Cooper pairs. One basic assumption under the BCS theory is the presence of a forbidden energy gap delta in the energy spectrum of a superconductor. The gap of the order of kTc is centred around the Fermi energy. For a critical temperature around 10 K kTc is about 1 meV. The gap is due to an attractive interaction between two electrons at energies close to the Fermi energy. Such interaction leads to a forming of bounded pairs, each of them composed by electrons of opposed spins and opposed moments. At the absolute zero all electrons are coupled in Copper pairs, increasing the temperature, electron pairs start to depair and to fill the energy levels above the gap. Electrical resistance in normal metals is connected to the scattering of electrons by impurities or the vibrations of the crystal lattice. Copper pairs, in comparison, do not interact with the crystal lattice vibrations. As a result, they can move without friction.

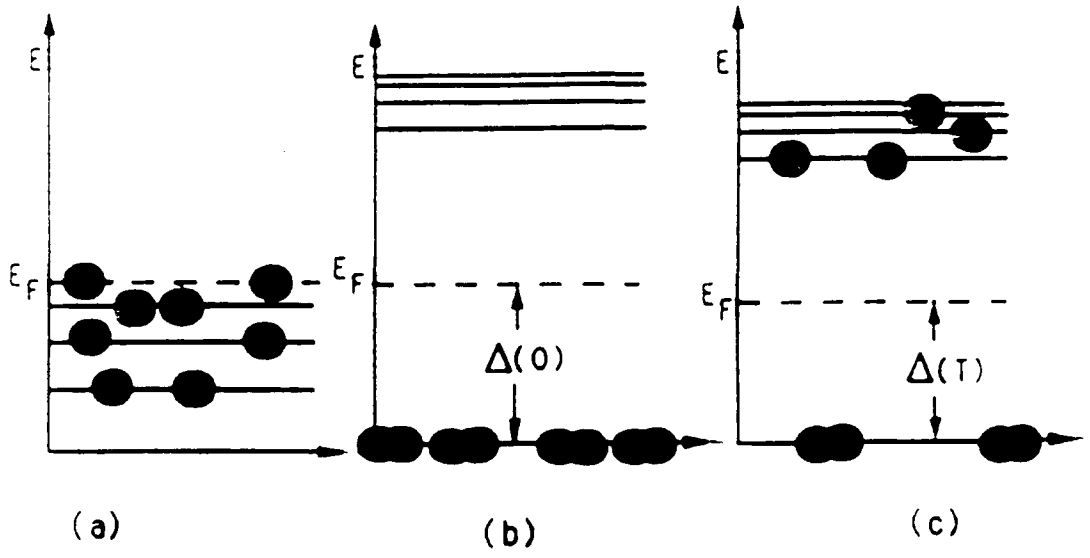

Fig. 1-6 *Energy spectrum [12] for*

a) a normal metal

b) a superconductor at T =0K

c) a superconductor at T ≠0K

1.4 Two different approaches: Bulk Niobium resonators and sputter-coated resonators

Superconducting RF cavities for electron machines are usually made of Niobium sheet material. Niobium combines the three important characteristics this application requires, namely good mechanical quality, high thermal conductivity at low temperature and a Tc of 9.25 K, the highest transition temperature among natural elements. The form is usually realised by welding together half-cells produced by deep drawing or spinning. The welding leads to a decrease of material quality in the vicinity of the welded zones and is , in addition, rather costly. Recently a technique to form cavities without any weldings is developed, based on the traditional lathe spinning.[13]

The accelerating field which can be obtained in bulk niobium cavities is often limited by quenching, field emission, or by global thermal instability. At high accelerating fields, the power absorption by local resistive defects are great enough to drive the neighbouring superconductor into the normal state, resulting in a sudden dissipation of the stored RF power (quench). To avoid thermal breakdown great efforts have been made to improve the Nb purity[14], in order to increase its thermal conductivity at liquid helium temperature. An alternative solution is the use of copper as cavity construction material. OFHC-copper has a thermal conductivity between 5 and 10 times higher than that of high purity Nb (RRR = 300). The Residual Resistivity Ratio (RRR) is the ratio of resistance at room temperature to the resistance just before transition into the superconducting state. It is proportional to the electron mean free path in metals at low temperature.

The cavity is coated internally with a superconducting film. Good results have been achieved with Niobium as coating material, but also other solutions are imaginable. The experience made with sputter-coated cavities in CERN shows, that higher Qo values are obtained in comparison with bulk Nb cavities.[15] Unfortunately they show also a larger Qo degradation with increasing accelerating field. Experimental it is seen that cavities with films of higher purity (RRR = 35 instead of 15), i.e. films with larger grain size, presents a larger decrease of slope without a noticeable reduction of the initial Qo value.

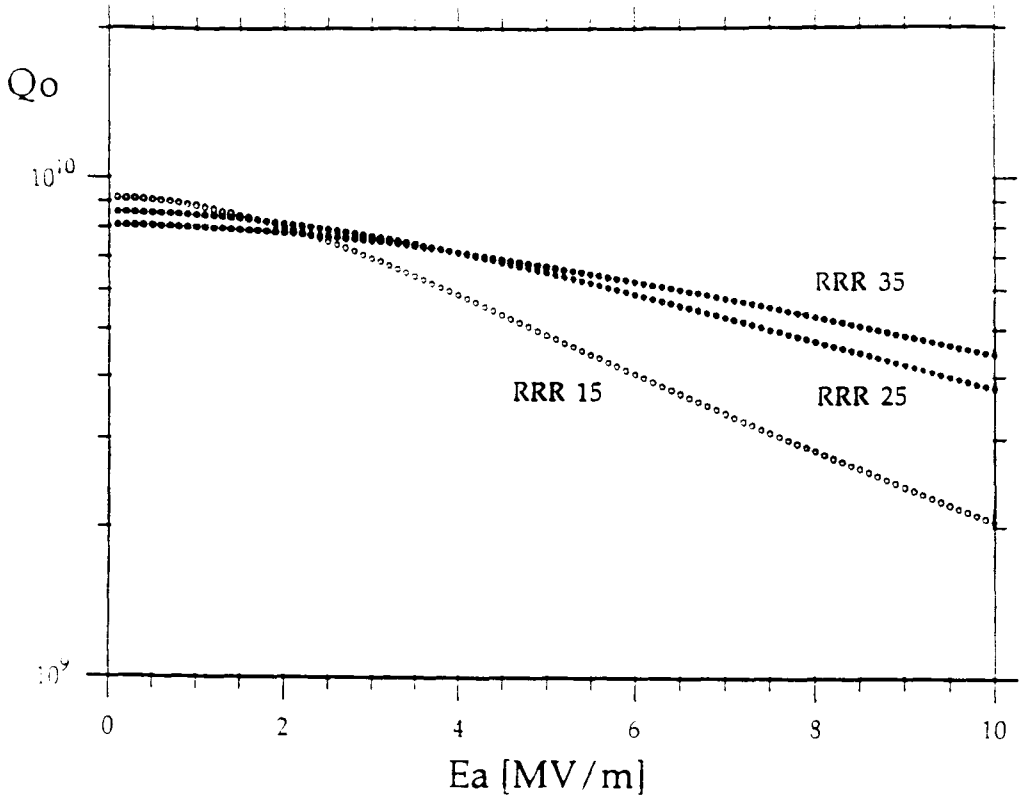

Fig. 1-7 *Qo as a function of the accelerating field* [16]

Another uncontested advantage of sputter-coated cavities is the insensitivity against trapped magnetic fields. When a cavity undergoes transition to the superconducting state in the presence of an external magnetic field, the magnetic flux gets trapped in a fraction of the surface area . This area remains normal conducting and as a reason, the Qo value can be reduced up to 50%. To avoid this effect, the earth magnetic field must be shielded during the cooldown. Nb coated cavities, on the contrary, are practically insensitive to external magnetic fields.

Furthermore sputter-coated cavities made of copper opens the way to save money for one of the most expensive part of an accelerator. For conventional cavities the compulsion to use high purity Nb rises the material costs. In the future the applicability of other coating materials with higher critical temperatures opens the way to increase the cooling temperature and to leave the cooling with superfluid Helium.

1.5 Literature results about sputter-coated 1.5 Ghz resonators

At CERN 1.5 GHz resonators are coated by DC cylindrical magnetron sputtering.[16] Before the first coating of a cavity they have investigated Nb films are produced under similar deposition conditions as in the real cavity. The best values they have reached are RRR = 20 and a Tc = 9.2K. The deposition rate at the equator position are in the range of $7As^{-1}$ from a power of 0.7 kW. Prior to the coating they mounted the cathode inside the cavity under clean air and baked the sputtering system at 200°C during the pump down. The residual pressure before deposition was $3 \cdot 10^{-7}$mbar. To obtain a homogeneous thickness of the film, the cavity was coated in 9 steps. The first discharges were done in the two beam tubes to getter the residual gases in a region which is exposed only to small RF fields. Than the cell was deposited with a thickness of about 5 µm. To displace the dense region of the glow discharge a movable permanent magnet of 4 cm length was used. The cavities reached Qo values at low fields of 10^{10}. After high pressure water rinsing to remove dust and particles from the surface they improved the Qo up to $3 \cdot 10^{10}$. At accelerating fields of 14 MV/m the Qo decreased to 10^9 at 1.6K.

In Japan at KEK laboratories[17] there has been researched and fabricated 1.5 GHz niobium coated copper cavities since 1989 in collaboration with Kobe Steel, Ltd. and Nomura Plating Co, Ltd. As coating method RF diode sputtering and magnetron sputtering was applied. The RF magnetron sputtering was carried out for one hour at a power of 1000W at an argon pressure of 2.7 Pa. This results in a film thickness of 2µm at the equator, 3~4 µm at the iris, and 1~1.2 µm at the cut-off tubes. The RF diode sputtering for 2 hours at 1000W at 2.7 Pa produces a niobium film thickness of 0.2 µm at the equator, 1~1.5µm at the iris, and 1.5~2.0 µm at the cut-off tubes.

The critical temperature (Tc) of niobium films on the sapphire substrates range between 8.5 K at the equator and 9.9 K at the cut-off tubes for Diode sputtering and about 9.7~9.9 K for the magnetron sputtering. The residual resistivity ratio (RRR) for Diode sputtering was between 3 and 7 and in the case of magnetron sputtering ranges from 8 at the equator to 20 at the iris. The high critical temperatures are impossible

for Nb as a pure element. The reasons could be a bad calibration of the temperature measuring system or a forming of NbC crystals due to contamination of the film by residual gases. Indeed, Auger electron spectrocopies revealed that at the film surface of about 10nm thick a large content of impurities, O, C and N was present. Far from the surface the impurity content was lower. This could be caused by the adsorption of the residual gases after sputtering. The Qo values at low power of 1.5GHz single cell coated cavities were measured at Kobe Steel, Ltd. The Qo at 4.2 K were below $4 \cdot 10^7$ in the initial stage. After the sputtering conditions were optimised, the Qo at 4.2K was improved to $5{,}4 \cdot 10^8$ at 4.2K. The cavity achieved a Qo of $2.1 \cdot 10^9$ at 1.8 K. The surface resistance was 500 nΩ. After the oxidised layer, about 50 nm thick, was removed by oxipolishing, the surface resistance decreased to 120 nΩ. The maximum accelerating field gradient was higher than 10 MV/m without any field emission or thermal instability.

2. Materials

2.1 R.f. Surface Resistance

When a rf electromagnetic field is oscillating in a cavity, only the electrons within a thin surfacial layer d (skin depth) of the resonant walls are interacting with the radiofrequency fields. The losses processes are so confined in a surfacial layer. For normal conducting materials according to the theory of skin effect, the skin depth δ is equal to

$$\delta = \sqrt{2/\mu\sigma\omega} \qquad (2.1)$$

where r is the d.c. conductivity at the working temperature and u the magnetic permeability of the cavity wall. The power losses produced in this thin layer are proportional to the surface resistance

$$Rs = \sqrt{\mu\omega/2\sigma} = \rho/\delta \qquad (2.2)$$

At finite temperatures the surface resistance is equal to the ratio of d.c. resistivity and the skin depth δ. Due to the fact that the Quality factor increases with decreasing surface resistance, one might expect, that higher Q-values are obtainable when building them of cooper from higher purity. Unfortunately due to the anomalous skin effect, the rf losses do not follow the $1/\sqrt{\sigma}$ law. At high frequencies the electron mean free path l becomes comparable to d and the relation between current and field $J=\sigma E$ is not valid any more. The existence of the anomalous skin effect prevents further energy losses reduction by improving the metal purity. This means that the most promising way to increase the Quality factor is the use of superconducting materials. The d.c. resistivity of superconductors is zero; but at frequencies $\omega \neq 0$, however they present a surface resistance about five orders of magnitude lower than for normal materials. The losses are caused to the penetration of the r.f. field in the surface of the superconductor. The normal electrons will be accelerated and decelerated by the field and interact with the lattice according to the anomalous skin effect.

In the framework of the BCS theory the surface resistance of a superconductor is given by

$$R_{BCS} = A\sqrt{\rho}\omega^2 e^{-aTc/T} \qquad (2.3)$$

with a=s/2, where s is the so-called strong coupling factor (usually 3.54; for Nb around 4). Since R_{BCS} depends on the square root of d.c. resistivity δ, a good superconductor for rf application must be as much "metallic" as possible in normal state, just before transition. Due to this formula one might expect, that at T=0K the surface resistance vanishes, but unfortunately in practice this behaviour has never been verified. At certain temperatures below Tc the resistance goes towards a constant value. this means the real surface resistance is the addition of BCS losses plus the so-called "residual losses".

$$Rs = R_{BCS} + R_{res} \qquad (2.4)$$

The reasons for these losses are not completely understood, but it seems to be sure. that accidental mechanism like dust, impurities or surface defects plays a crucial role.

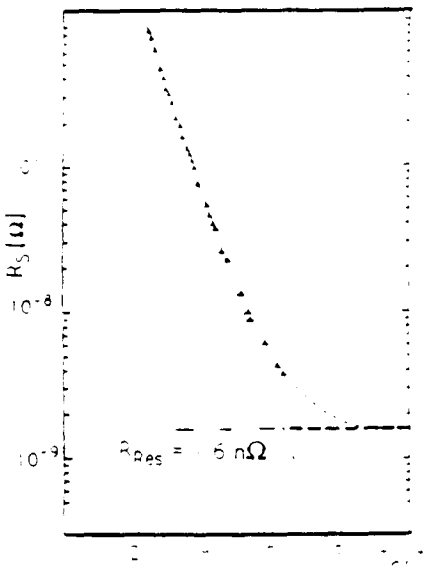

Fig. 2-1 *A classical picture for the residual surface resistance. The dashed line is the residual term, while the continuous line is the BCS predicted surface resistance* [12]

The sources of residual losses which are more investigated and discussed are the following:

a) Losses due to a non-ideal surface quality[18]

In general, the non-controllable nature of this kind of losses makes them rather difficult to analyse. But it is universally recognised that the worst polished superconducting surface show the highest residual losses. Inclusions of metallic foreigner particles into the superconductor within a penetration depth from the surface can also be source of Joule losses. Depending on the thermal conductivity of the superconductor and on the thermal resistance between the normal particles and the superconductor, normal areas will dissipate more and more power, while temperature increases. As a result the critical field gets lower and lower. All this can result into a sudden transition from the superconducting to the normal state (quench) and can be a severe limitation to the achievement of high fields inside superconducting resonators.

b) Losses due to an Oxide layer present on the surface[19-21]

It must be kept in account that the only two superconductors most widely used (i.e. mounted in rf structures on real accelerators) for superconducting cavities are Lead and Niobium. Without doubt when high performance resonators are required, the Niobium choice becomes compulsory. From the surface stability point of view niobium is superior to lead: Lead has several stable oxides; Niobium has only two oxides Nb_2O_5 and NbO. Due to the small thickness of saturation, NbO plays a minor role in the mechanism of rf losses. Nb_2O_5 also is recognised to be not significant, since for example, only fractions of $n\Omega$ are expected in a 6 nm Nb_2O_5 layer without defects. On the contrary a possible source for residual losses can be represented by the interface suboxide, mainly between Nb grains and NbO. An Oxygen content of only 1at. % dissolved inside Niobium indeed reduces the critical temperature Tc by 10%.

c) Losses due to the superconductor polycrystallinity[22]

For type II superconductors the rf and microwave surface impedance can be strongly limited by dissipative process determined by the intergranular coupling. Additional surface resistance can indeed arise

due to the nature of grain boundaries behaving as semipermeable walls for rf waves.

d) Losses due to Hydrogen segregation[23]

A serious kind of additional losses has been recently recognised to be a potential enemy to fight. It is well-known that Niobium, if electro-polished or chemically treated by immersion can be charged at least on the surface by hydrogen. Hydrogen mobility in niobium is known to be very high; moreover it is clear that if diffusion there is , it will happen through grain boundaries.

2.2 A15 Materials

The stoichiometry of the A15-Materials is A_3B. The B-atoms form a body centred cubic lattice, and the A-atoms are arranged pairwise on the cubeedges, parallel to the coordinate axes.

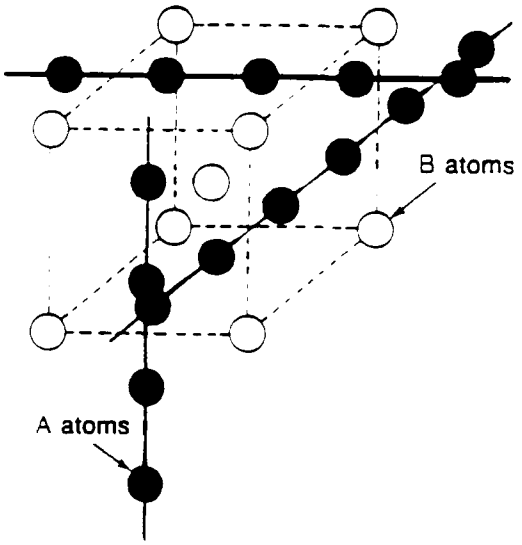

Fig.2-2 *Crystal structure of A15-compounds* [8]

A typical feature of this structure is, that A atoms make up families of intersecting linear chains. the distance between the atoms within one

chain being the shortest distance between the atoms in the A15 structure and being 22% less than that between A atoms belonging to different chains. The A-atom always constitutes a transition element of groups IV, V or VI (Ti, V, Cr, Zr, Nb, Mo, Ta, W), whereas the B atom may be represented either by a nontransition element or a transition element.

From the phase diagrams of 28 compounds with A-15 structure the A_3B compounds may be divided into two groups, according to their regions of homogeneity are formed. The first group comprises compounds whose region of homogeneity is practically absent or extends only in the direction rich in the A component (V_3Si, V_3Ga, V_3Ge, V_3Au, Nb_3Ga, Nb_3Ge etc.). They are called "typical" by convention. In "typical" A15 the maximum values of Tc are obtained near to stoichiometric composition and at high degree of order. Such a situation is thought to be associated with the conservation of the integrity of the linear chains in an A15 structure. The other group of compounds, which are called "atypical", contains compounds whose region of homogeneity extends towards the B component or in both directions from stoichiometric composition (Mo_3Ir, Mo_3Pt, Cr_3Os, V_3Ir etc.). In these compounds (having lower Tc) atoms in the chains are likely to be replaced by B atoms and integrity is not conserved. In Table 2-1 data on superconducting transition temperatures in compounds with A15 structure are presented.

B \ A	Ti	Zr	Hf	V	Nb	Ta	Cr	Mo
Al				11.70	18.80			0.58
Ga				15.9	20.3		<0.35	0.76
In				13.9	8.8-9.2			
Tl	<0.35	<0.35		<4.20				
Si				17.1	18.0-19.0		<0.015	1.70
Ge				11.2	23.2	8.0	1.20	1.8
Sn	5.80	5.93		12.3-17.9	18.0	8.35		
Pb		0.76		<4.2	8.0			
P				<1.00				
As				0.20				
Sb	6.5	<1.20		0.80	2.0	0.72		
Bi		3.4		<4.20	3.0			

Table 2-1 Tc in compounds with A15 structure [24]

This Table shows, that the highest Tc for A_3B compounds of Vanadium and Niobium are obtained in those cases when the B-atom is represented by a nontransition element Al, Si, Ga, Ge, Sn. At deviations from stoichiometry and with the degree of long-range order S one can see that Tc is very sensitive to these effects. For example, in the compound V_3Si of stoichiometric composition Tc varies from 16.85 to 17.1K, whereas at 20.1% Si Tc is 9.4 K.[25]

Phase Diagrams

The knowledge of the precise limits of stability of the A15 phases is very important since in many of the particularly interesting systems the superconducting and normal-state properties depends critically on composition. If in a binary system an A15 phase occurs, this phase always immediately follows BCC solid solution with increasing concentration of the B component. On the higher concentration side, the A15 phase is often followed by phases exhibiting the tetragonal sigma structure (e.g. Nb-Al) or the tetragonal W_5Si_3-type structure (e.g. Nb-Ge). Under the A15 compounds with a Tc>15K there are only V_3Ga, V_3Si and Nb_3Sn which are stable at the stoichiometric composition, whereas Nb_3Al, Nb_3Ge and Nb_3Ga are metastable and can only produced with an excess of niobium.

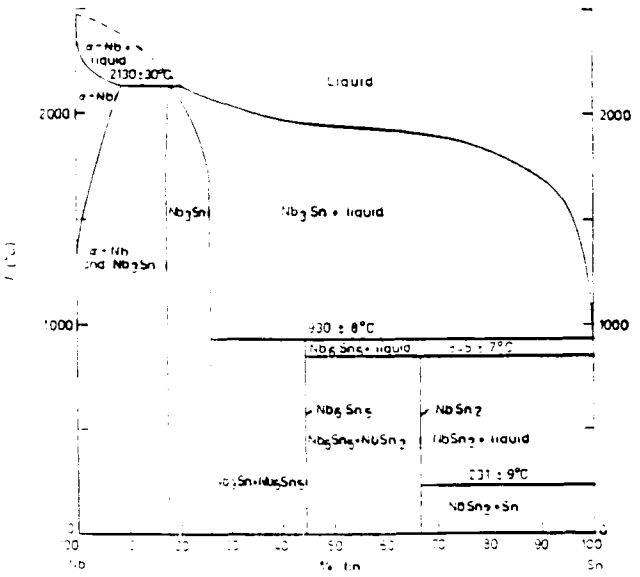

Fig. 2-3 *Phase diagram of Nb_3Sn* [26]

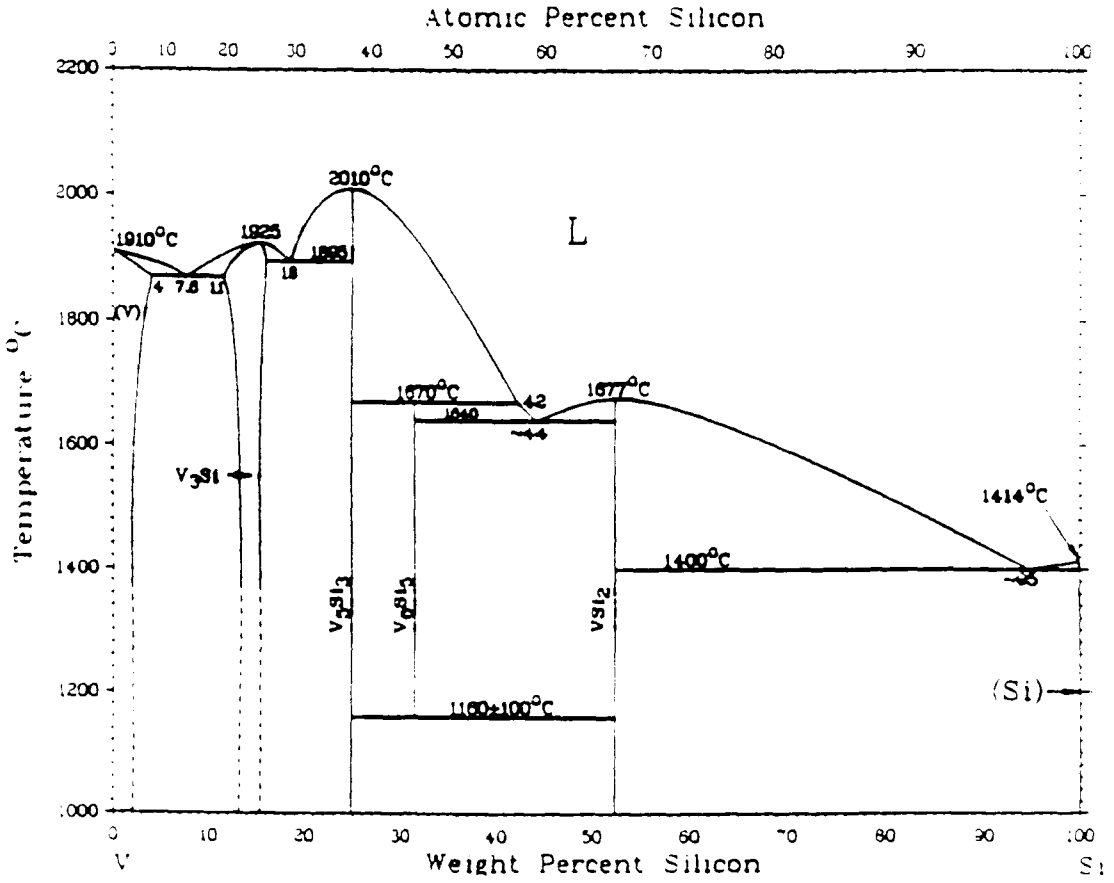

Fig. 2-4 *Phase diagram of V_3Si* [27]

Dependence from Tc versus Ne

Analysis of different empirical criteria of superconductivity shows that a clear correlation occurs between Tc and Ne; i.e. the mean number of valence electrons per atom. In fact, it follows from consideration of Fig. 2-5 that the superconductors with lower values of Tc group near two electron-concentration intervals: 4.50 to 4.75 e/a and 6.25 to 6.60 e/a .

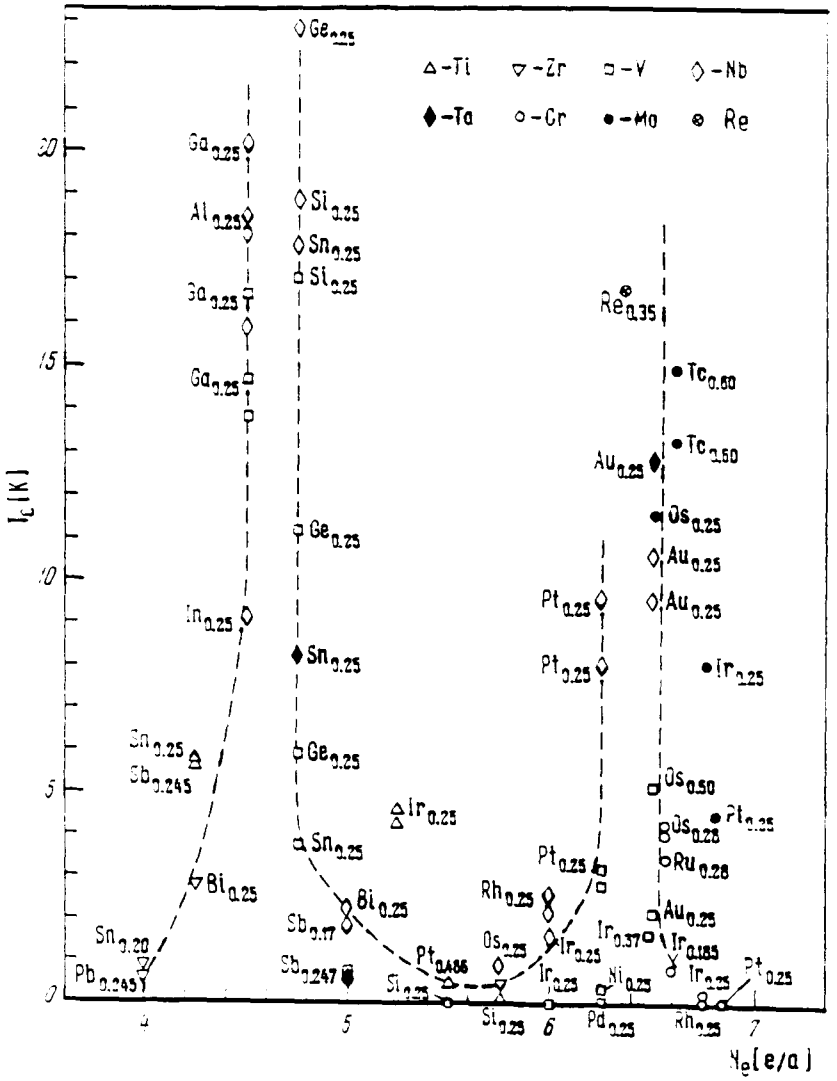

Fig. 2-5 *The superconducting transition temperature of A15-compounds as a function of electron concentration Ne* [28]

The first range encompasses compounds whose B element is not a simple metal, and in the second region the B-atoms are transition or noble metals. In the region of the first peak two groups of A15-compounds with the same electron concentration stand out: either 4.50 e/a (Nb_3Ga, Nb_3Al, V_3Ga, V_3In, V_3Al, Nb_3In) or 4.75 e/a (Nb_3Ge, V_3Ge, V_3Si, Nb_3Sn, V_3Sn). For A_3B compounds, Fig.2-6 and 2-7 carry values of electronic heat capacity and paramagnetic susceptibility as functions of Ne.

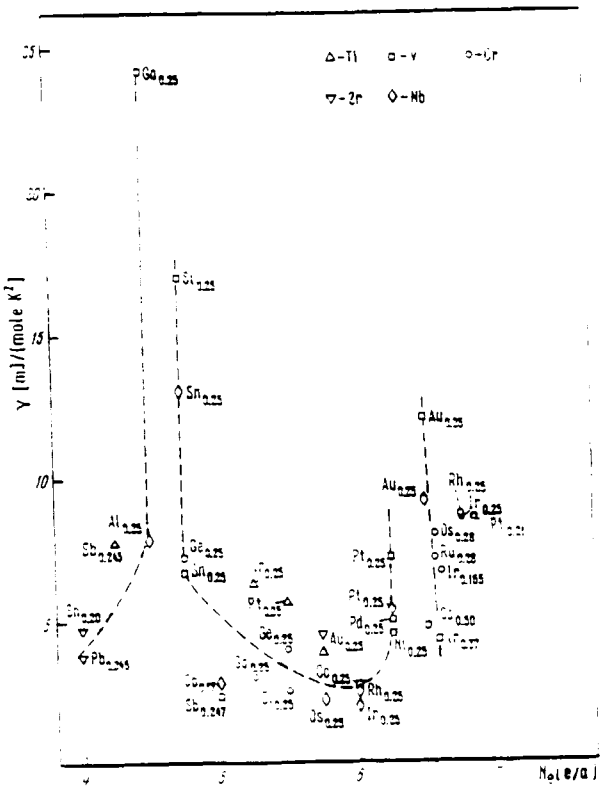

Fig.2-6 *The electronic heat capacity of A15 compounds as a function of Ne* [29]

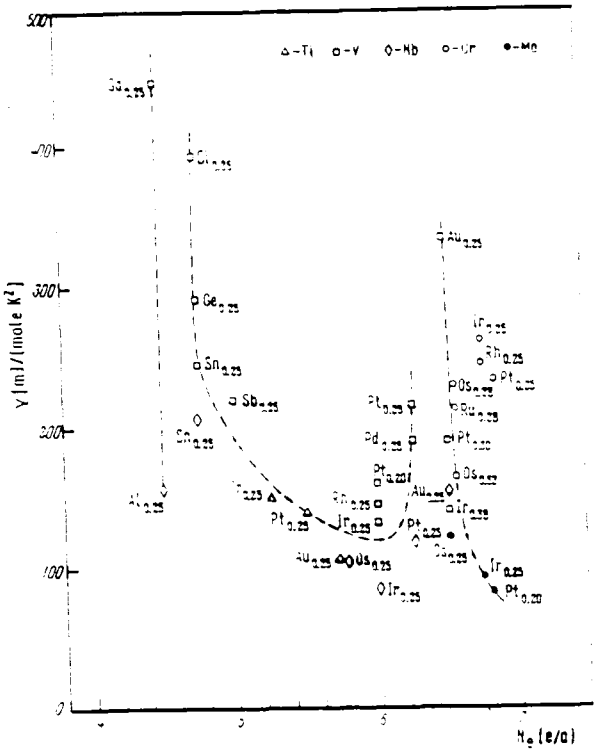

Fig.2-7 *The paramagnetic susceptibility of A15 compounds as a function of Ne* [30]

One can readily notice a certain similarity in the character of the variation of these properties with the dependence of Tc on electron concentration. The relative arrangement of points coincidences in all three figures, except in rare cases. Since both, the electronic heat capacity and the paramagnetic susceptibility in metals is proportional to the density of states on the Fermi level, the presence of the above correlations gives good reason to conclude that high values of Tc in A15 compounds are accompanied by a higher density of states on the Fermi level. Indeed one can see from band structure calculations carried out by Klein[31] that there is a sharp peak in the density of states close to the Fermi energy in the case of V_3Ga, V_3Si and Nb_3Sn.

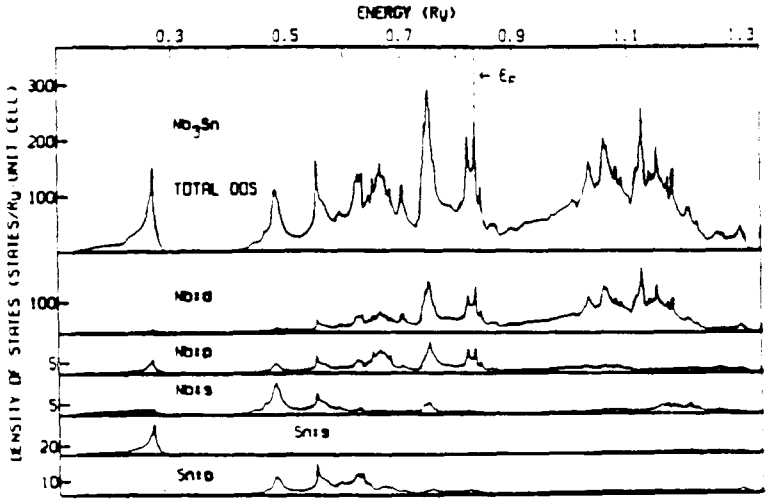

Fig. 2-8 *Densities of states of Nb_3Sn* [31]

3. Experimental Technique

3.1 The glow discharge

If a dc voltage is applied between two electrodes with the distance d in a gas at low pressure 10^{-2} - 1 mbar, a small current will flow between the electrodes. It is caused by a small number of ions and electrons, which always exists in a gas due to ionisation by cosmic radiation. With increasing the voltage, the electrons reach energies which enable them to ionise atoms by collision, each ionisation process produces further electrons. The ions, that result from these collisions, are also accelerated by the applied field and move toward the cathode. When striking the cathode they can release secondary electrons. The secondary electron emission ratio of most materials is of the order of 0.1 so that several ions must bombard a given area of the cathode to produce another secondary electron. Initially, the bombardment is concentrated near the edges of the cathode . As more power is supplied, the bombardment covers the hole surface and a constant current is achieved. Further increase in power produce both increased voltage and current in a region known as the abnormal glow discharge. This mode is usually used in sputter deposition techniques. The two processes of ionisation by electron impact and secondary emission of electrons by ions thus control the current I in the system. If each electron, according to the Townsend criterium

$$y \cdot e^{(\alpha d - 1)} = 1 \qquad (3.1)$$

produce more than one new electron, the glow discharge burns self-sustained. This happens by the breakdown voltage, which is a function of the product of the pressure p and the electrode distance d (Paschens law).Within a glow discharge there exists distribution of potential, field, space charge and current density. Visually these are seen as regions of varied luminosity, as shown in Fig. 3-1.

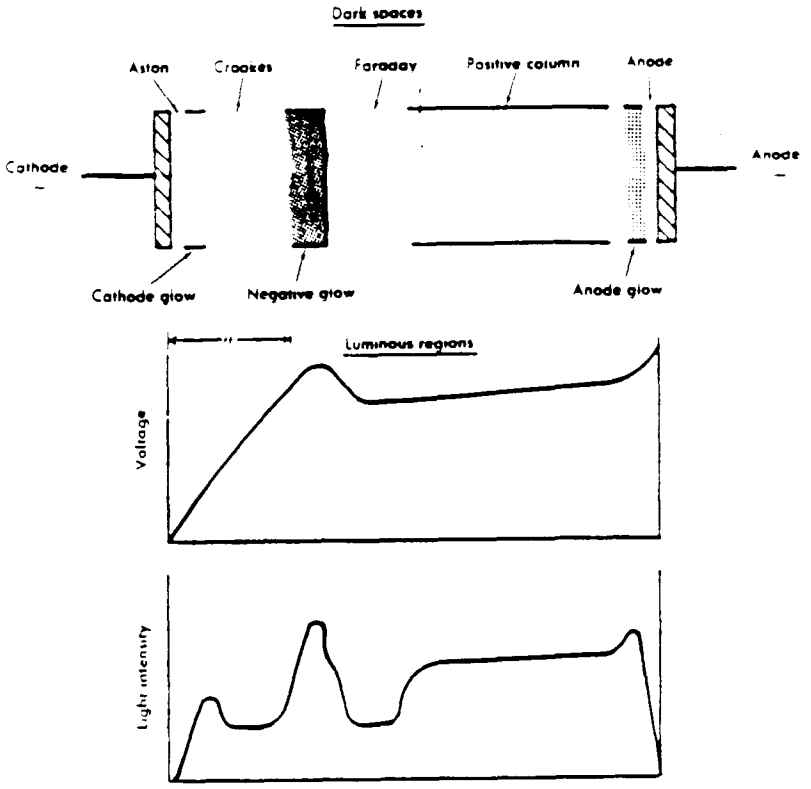

Fig. 3-1 *Appearance of glow discharge at low pressure* [32]

The various luminous and dark regions of a glow discharge arise in the following manner: Electrons usually leaves the cathode with small velocity, the energy is of the order of one electron volt. They are not able to ionise gas molecules until they are accelerated to sufficient energies. This results in a region called "Aston's dark space". The cathode glow is the region in which the electrons reach energies corresponding to the ionisation potential, and this is the luminous region closest to the cathode. In the "Crookes' dark space ", the electron energies are over the maximum excitation potential, so that no visible light is emitted. When the negative glow is reached. the number of slow electrons (i.e., those produced by an ionising collision) has become very large. These electrons do not have sufficient energy to produce ionisation, so they do possess enough energy to cause excitation and are the cause of the negative glow. The "Faraday dark space" and the positive column are nearly field-free regions and are characterised by nearly equivalent numbers of ions and electrons. Unfortunately, for glow discharges applied as sputtering sources, the electrode separation needs to be small so that the anode is

located in the negative glow. Therefore, the positive column and the Faraday dark space not exist.

3.2 The sputtering technique

Sputtering is the mechanically outknocking of atoms or molecules from the surface of a target with energetic ions. The sputtered atoms can condense on a substrate to form a thin film. The simplest configuration to create a sputtering source is the Diode sputtering configuration (Fig.3-2). It consists of a vacuum chamber in which between two electrodes an anomalous glow discharge will be created. The negative electrode (cathode) presents the target, whereas the substrate is placed on the anode.

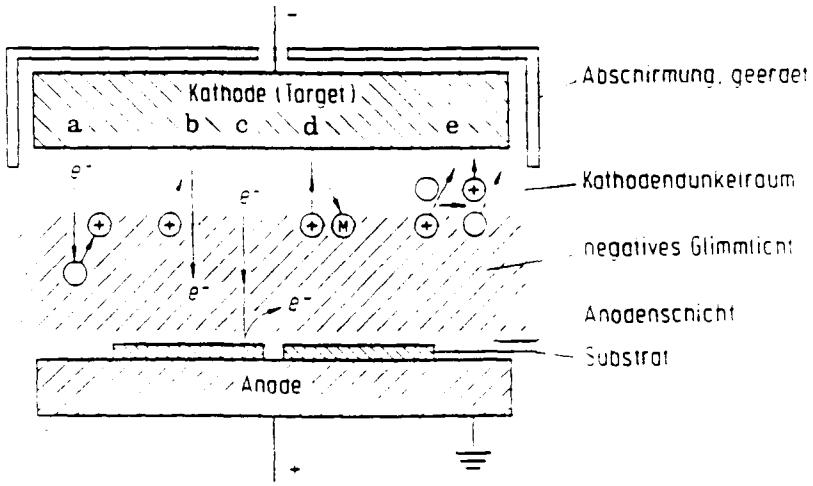

Fig. 3-2 *Configuration of a Diode Sputtering Source* [33]

After evacuation to high vacuum the chamber is filled with the sputtering gas, usually Argon, at a pressure of 10^{-2} - 10^{-1} mbar. The discharge is created by applying a dc voltage of 1-5 kV between cathode and anode. The argon gas will be ionised and accelerated towards the cathode, where they extract atoms from the target surface. The sputtered atoms diffuse in the chamber following the $\cos^{-1}$ law and finally condense on a surface. The kinetic energy of the atoms released is a few eV, i.e. substantially higher than that of evaporated atoms (kT=0.1 eV at 1200 K). These higher energies lead to a better adhesion and higher density of the film. Almost every material can be sputtered, independent of the melting

point or other physical properties. The number of released atoms per impinge ion is called the sputtering yield.

The yield depends on the following parameters:

Material: The yield Y is by a given species and energy of the ions reciproce to the sublimation enthalpy of the target material (Y / E_0).[34]

Energy: The sputtering process starts at a threshold energy E_{thres} of 10-30 eV, and increasing linear with increasing ion energy. At energies from 10^4 eV the sputtering yield reaches a bride maximum and after that it decreases because of ion implantation effects.[35]

Ion mass: The variation of the ion species at constant energies shows. that the sputtering yield has a maximum, when the ion mass M_i is approximately equal to the mass of the target atoms M_t.[36]

Incident angle: The sputtering yield increases with growing incident angle Ω proportional to cos Ω^{-1} law due to the smaller change of impulse by greater angles. With values of Ω near 90° the effect of ion reflection becomes dominant and Y decreases.[37]

3.3 The Magnetron sputtering

Magnetron sputtering sources can be defined as diode devices in which magnetic fields are used to increase the ionisation efficiency of the electrons. The effect of the magnetic field is to increase the distance the electrons have to travel by the forming of electron traps, thus increased the probability of collisions. As a consequence. very high degrees of ionisation are possible with relatively low pressure (in the range of 10^{-3} mbar). The magnetic field is shaped in a way to get a plasma confinement. Electrons can be trapped by a magnetic and/or electrostatic mirror. However, a general statement for magnetron constructions is that magnetic field lines must "be born from the cathode and die onto the target"[38]. The high degree of ionisation allows higher deposition rates at lower voltages in comparison to "normal" sputtering sources. The high

current density leads to a strong heating of the target, to prevent this it is necessary to cool the sputtering head.

Generally the magnetron sputtering sources can be planar or cylindrical formed. Cylindrical configurations can be post magnetrons or hollow cathodes (Fig.3-3). In the first case the inner cylinder is the cathode and the outer cylinder the substrate, in the latter case it's vice versa. In both cases it's needed to prevent plasma losses by cathodic wings at the end of the cylinders. The main advantage of cylindrical magnetrons is the uniform erosion of the target material. Typical working conditions for copper sputtering are: deposition rate 200nm min^{-1} and p = 10^{-3} mbar, B = $2.5 \cdot 10^{-2}$ T, j = 200 Am^{-2}, U = 600V.

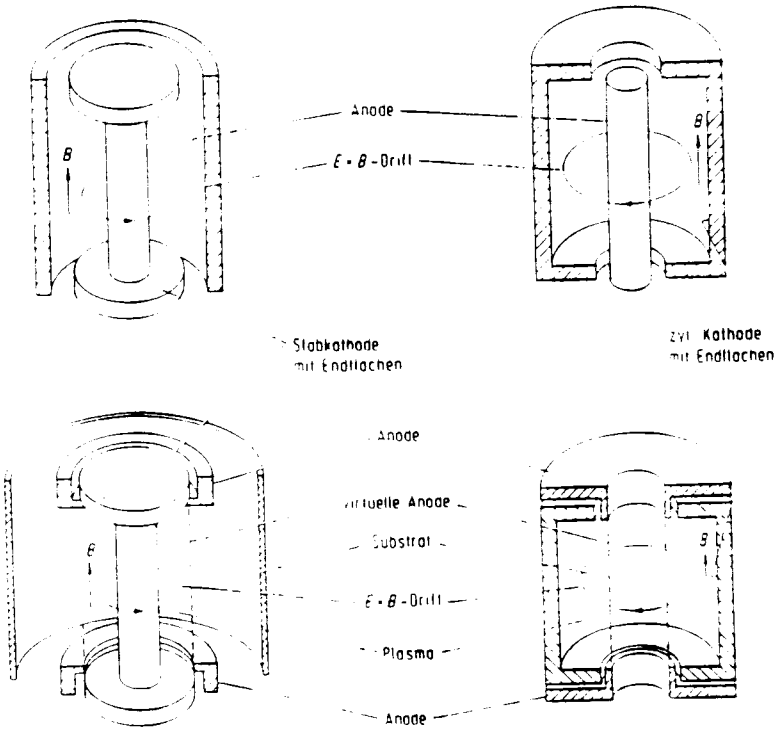

Fig. 3-3 *The configuration of cylindrical magnetron sputtering sources* [33]

The function principle of planar magnetrons are the same as for cylindrical once. but obviously they have another structure. Here the system consists of a planar cathode surface parallel to an anode. that serves as a substrate holder. The geometry can be disk shaped or rectangular. In any case the non uniform magnetic field leads to an unsymmetrical erosion of the target material.

Electron transport processes

The homogenous magnetic field axial to the cylinder in the range of 10^{-2} T does not influence the ions, but only the electrons. The electrons will drift along the magnetic field lines and orbit them with a giro frequency ($wc=1{,}76 \cdot 10^{11}$ B). The electric field E perpendicular to the magnetic field leads to a E X B drift with the speed $v \cdot c = E \times B/B^2$.

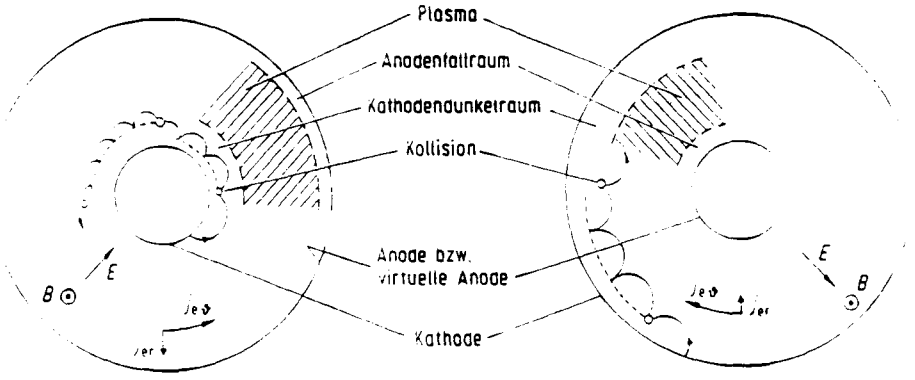

Fig. 3-4 *Electron transport processes in a cylindrical magnetron* [33]

3.4 Film structure

Film growing

Any thin film deposition process involves three main steps:[39]

- The production of the appropriate atomic, molecular, or ionic species
- The transport of the coating species to the substrate through a medium
- The adsorption/condensation of these species onto the surface of the substrate

The general picture of the step-by-step growth process can be described as follows: The coating species hit the substrate surface, lose their velocity component normal to the substrate (in the case of not to

high incident energy) and are physically adsorbed on the surface. The adsorbed atoms are not immediately in thermal equilibrium with the substrate and move over the surface. They interact with themselves, which leads to the forming of clusters. The clusters or nuclei are thermodynamically unstable and tend to desorb. If the growing process by interaction with adsorbed atoms is stronger than the desorbtion process, they grow until they reach the so-called nucleation stage, where they become stable. A nucleus can grow both, parallel to the surface by diffusion of the adsorbed atoms and perpendicular by direct impingement of incident atoms. In general, at this stage the lateral growth is much higher than the perpendicular. The grown nuclei are called islands. In the next step the islands start to coalence with each other, forming bigger islands. By increasing the surface mobility as, for example, with higher substrate temperature this tendency can be supported. Finally, all islands are connected to a porous network. A completely continuos film is formed by filling up the holes and channels of the network.

The growing of the islands is a randomly process, so that when they touch each other, grain boundaries and many point and line defects are incorporated into the film. These defects results in inherent stress and worse physical properties of the film.

Film structure

It is useful to distinguish the structure of physical vapour deposited thin films in three structure zones and one transition zone, each with his own characteristic features and physical properties.[40] The different zones are divided by the ratio of substrate temperature T to coating material melting point Tm. The low temperature zone 1 structure ($T/Tm<0.3$) was columnar, consisting of tapered units defined by voided growth boundaries of the type shown in Fig.3-5. The transition zone T in the region between zones 1 and 2 consisting of a dense array of poorly defined fibrous grains. The zone 2 structure ($0.3<T/Tm<0.5$) consisted of columnar grains, which were defined by metallurgical grain boundaries. The grain boundaries increased in width with increasing T/Tm in accordance to activation energies typical of surface diffusion. The high temperature zone 3 structure ($T/Tm>0.5$) consisted of equiaxed grains,

which increased in size in accordance with activation energies typical of bulk diffusion.

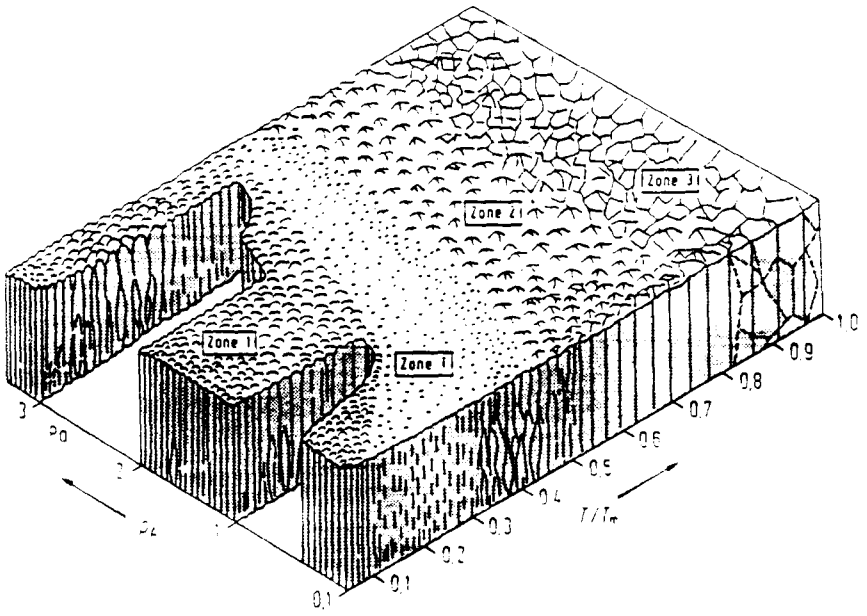

Fig. 3-5 *Structure zone model* [40]

3.5 Vacuum system

For the sputtering of high purity Nb films it is necessary to work with the highest possible cleanliness, since Nb is a strong getter material. Therefore ultra high vacuum has to be obtained in the sputtering chamber. Only little contents of Oxygen would lead to a decrease of the d.c. conductivity and herewith, according to formula 2.3 to a decrease of the critical temperature. Our system is equipped with a turbomolecular pump of 320 ls^{-1} pumping speed, prepumped by a rotary pump of 18 m^3/h. The turbomolecular pump has magnetic bearings to reduce the content of hydrocarbons to a minimum. All flanges are of conflat type, sealed with copper O-rings. Several vacuum gauges, namely a Pirani gauge, a Bayard-Alpert gauge and a Extractor gauge, offers a exact measuring in each pressure region. The Argon flow is controlled by a all metal dosing valve, which provides precise and reproducible gas inlet for very pure gases. It is bakeable up to 450° C. The ultimate pressure is better than 10^{-9} mbar after 48 hours of baking at 250° C.

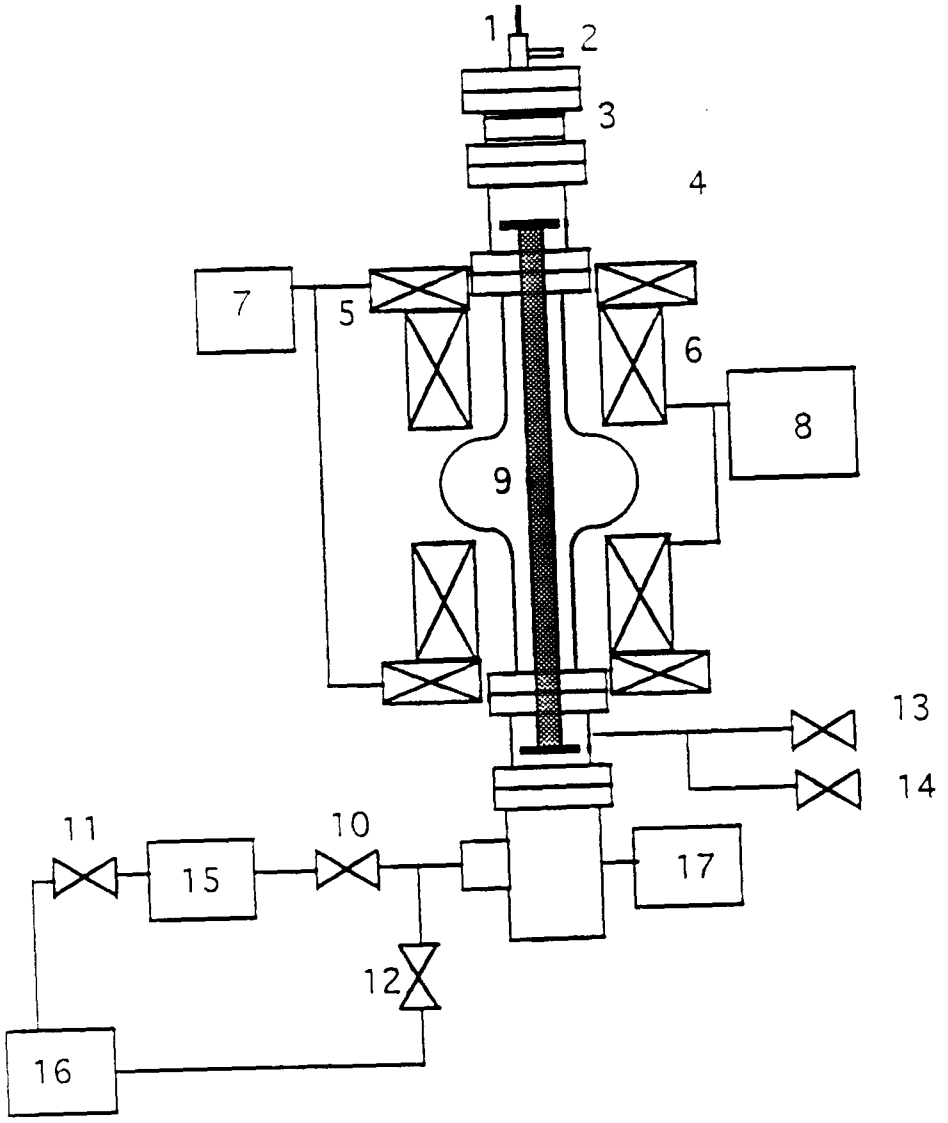

Sketch of the vacuum system

The numbers presents the following construction elements of the system:

1	Water input
2	Water output
3	Ceramic insulator
4	Target(Cathode)
5	Upper coils
6	Down coils
7	Power supply upper coils
8	Power supply down coils
9	Cavity
10	Main valve
11	Prepump valve
12	Bypass valve
13	Argon inlet
14	Nitrogen vent valve
15	Turbopump
16	Prepump
17	Measuring instruments

3.6 Configuration for 1.5 Ghz

The magnetron configuration consists of a columnar vacuum chamber, where the middle part is represented by the cavity. Inside this tube the cathode is placed, connected to the columnar by a ceramic insulating element. The cathode is made from Nb with a RRR better than 250. The high purity is needed to prevent contamination of the film by the cathode. During the sputtering process the cathode is exposed to a ion bombardment, which results in a strong heating. To prevent an evaporation or melting a water cooling is necessary. Since Nb can be oxidate the water flow takes place in an inner stainless steel tube. The disadvantage of this solution is a bad heat exchange between both tubes. Due to this, the cathode temperature rises estimately up to 1000° C and heat by radiation the cavity wall. For future experiments, the feasibility of a direct water cooling of the cathode will be tested. To provide nevertheless a constant temperature during the sputtering process a regulation system has been designed. It consists of a heating strip surround the cavity equator and 4 ventilators. With this method the desired temperature of 200° C can be hold in a range of 10° C. Higher substrate temperatures will surely increase the film quality, but unfortunately copper will become too soft (the cavity risks imploding) and strongly oxidises under those conditions.

As sputtering gas argon is chosen. The flow rate is controlled by a high precision leakvalve, connected to the chamber directly under the columnar part. This means that the main part of the gas will be immediately pumped and only a little fraction of the gas in the cavity will be exchanged. In this way the pollution from the argon gas, even when the cleanliness of the gas is 99.9999 % to the film is lower, resulting in higher film quality. The magnetic field is generated by external coils, as sketched in fig. 3-7

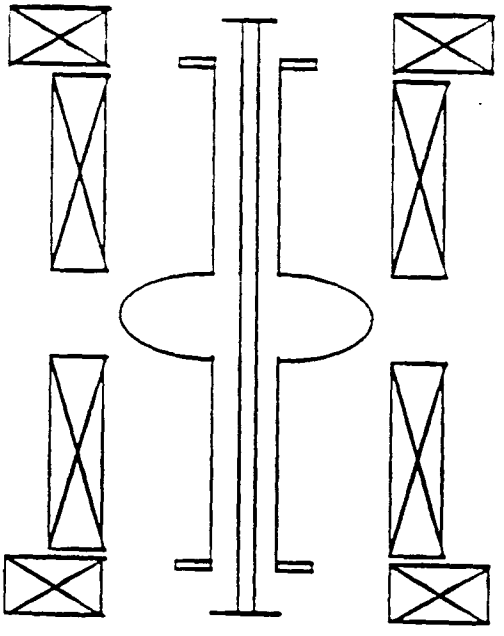

Fig. 3-7 *Cathode, cavity and coils arrangement in the DC post magnetron configuration*

The two long coils are needed for the plasma confinement: the two shorter help the electromagnetic mirror focusing the magnetic field on wings. In contrary to a standard cylindrical DC post magnetron, this configuration opens the way to create a special magnetic field distribution. With a common uniform magnetic field, the thickness and RRR distribution would be highly disuniform. Caused to the complex shape of the cavity, the thickness at the equator would be 10 times less than in the iris.

3.7 Volt-Ampere characteristics

The quality of ionization processes in a plasma discharge can be easily demonstrated by the help of the Volt-Ampere characteristic.[41] Discharges operating in the magnetron mode obey a V-I relationship of the form $I \sim V^n$, where n is an index to the performance of the electron trap and is typically in the range 5 - 9. To measure these characteristics we connect our sputtering source to a computer, which in every second takes the values of voltage and current and read them directly out on the

monitor. It is programmed to increase the current within 30s from 0 to 10 A. The measurings are made in two different modes:

- variation of Argon pressure at constant magnetic field (fig. 3-8 and 3-9)
- variation of magnetic field with constant Argon pressure (fig.3-10 and 3-11)

The magnetic field values presented in the following figures are calculated for a distance of 5cm from the center of the cavity.

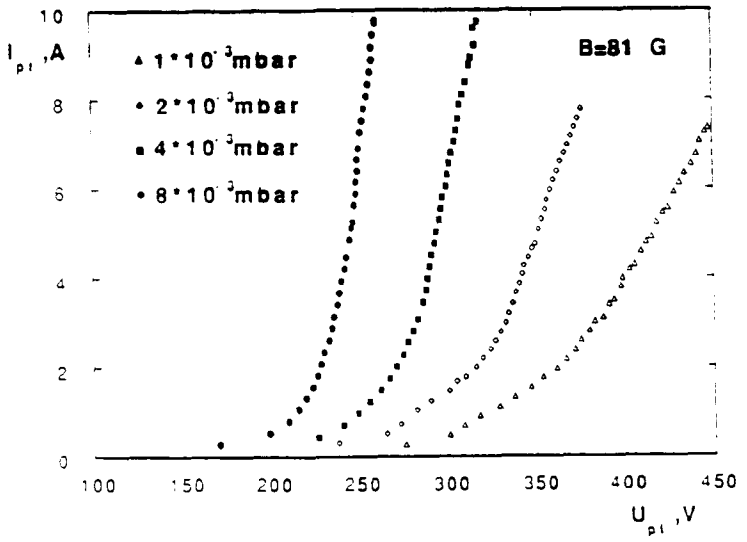

Fig.3-8 *Volt-ampere characteristics at constant magnetic field with variation of pressure*

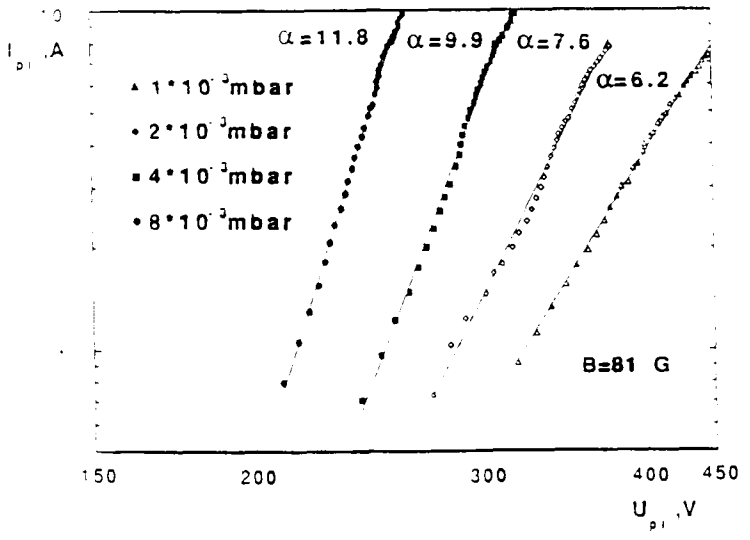

Fig. 3-9 *Volt-ampere characteristics at constant magnetic field with variation of pressure in logarithmic scale*

From fig.3-8 one can see that with increasing magnetic field the ionisation efficiency increases and the plasma becomes more dense. This is expressed in a stronger slope of the curve, i.e. in a strong increase of current by only a slightly higher voltage. Fig.3-9 shows the same dependence with logarithmic scales. The fit with the $I \sim V^n$ law give a value of 10 for a magnetic field of 108 G. In comparison with common cylindrical magnetrons this is a rather high value and prove that we reach our goal of strong plasma confinement in the center of the cavity. For lower field values, the voltage will increase abruptly without reaching high currents, as shown in fig 3-8 and 3-9 for 31 G. The values of n for these fields is 2, obviously not sufficient to reach high plasma densities.

Fig. 3-10 and 3-11 show the Volt-Ampere characteristics with pressure varying from 1.10^{-3} mbar up to 8.10^{-3} mbar by a constant magnetic field of 81G.

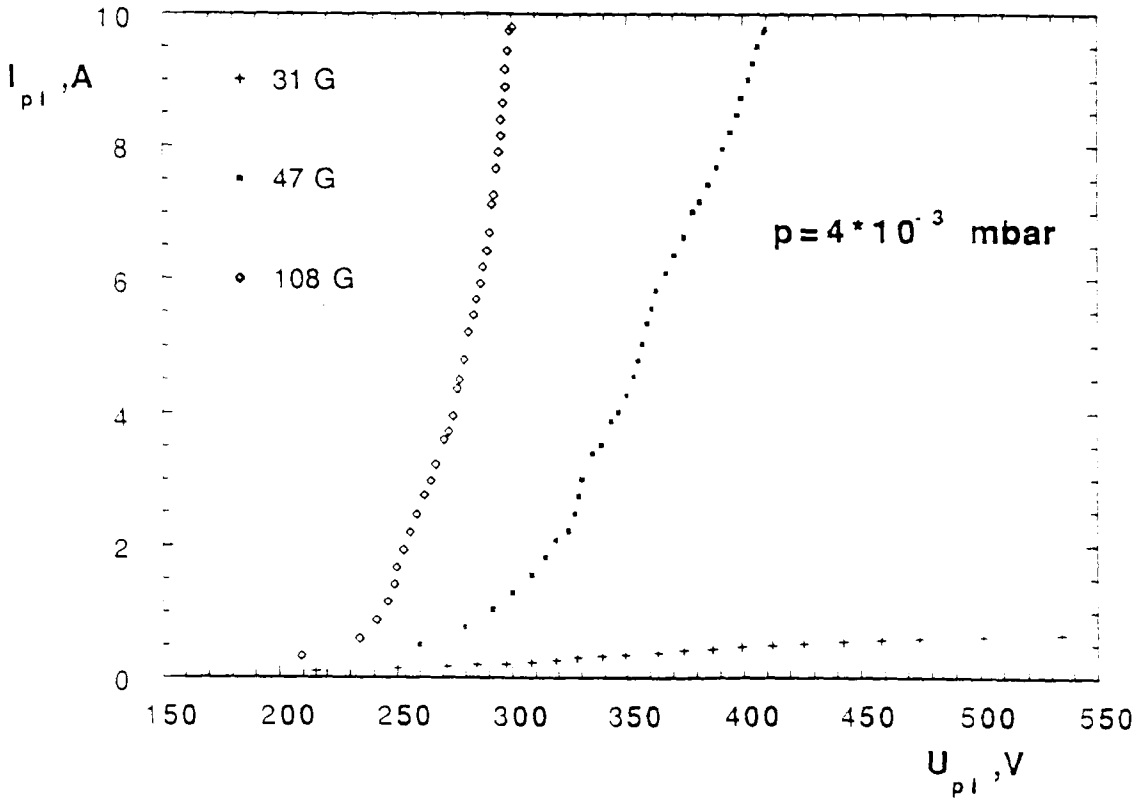

Fig 3-10 *Volt-ampere characteristics at constant pressure with variation of magnet field*

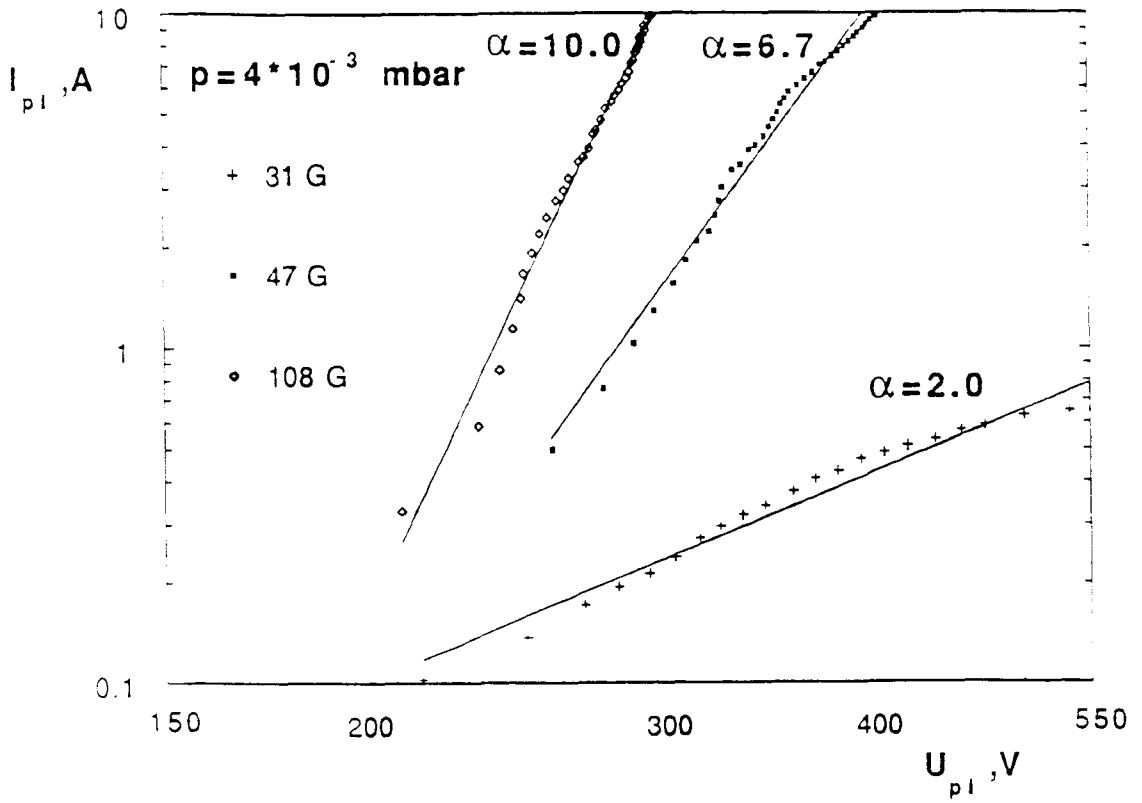

Fig 3-11 *Volt-ampere characteristics at constant pressure with variation of magnet field in loarithmic scale*

By pressures of 1 and 2 mbar the values of n are 6.2 and 7.6, i.e. rather low, whereas at pressure of 4 and 8 mbar the slopes of the curves are considerably higher, which indicates a good plasma confinement. At 8 mbar, however the voltage exceeds not 270V. Since in theory the film growing conditions are better at higher voltages the best compromise between good plasma confinement and sufficient voltage are about 4mbar. In fig. 3-12 the conditions of pressure and magnetic field strength are demonstrated, that permitted stable operation of the magnetron. One can see that a minimum magnetic field strength must be exceeded, even at relatively high pressures, to create a glow discharge. With increasing the magnetic field one can go to lower pressure operation up to a field strength of 60 G. When passed this value a further decrease of pressure is not possible, because the ionisation efficiency not increases any more.

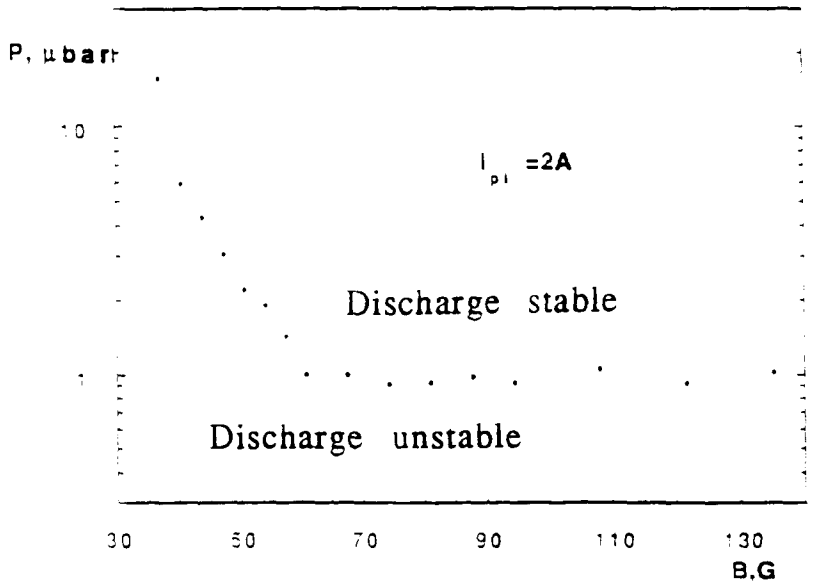

Fig. 3-12 *Conditions of pressure and magnetic field strength for stable operation of the magnetron*

3.8 Experimental results

To measure the properties of the films the following measuring techniques are used:

1. Film thickness measurements

The thickness is measured with the stylus method. The principle of this methode is as follows: A diamont needle with a tip radius of about 10 µm serves as electromechanic pick-up. The vertical movement of the needle, when it slides over the film substrate step, can be measured and directly read-out on a monitor. The measurement range spans from 200A to a few µm[42]. Presupposition for the application of this method is a sufficient hardness of the film and a plane surface.

2. Residual resistivity ratio measurements

The RRR of the Nb coatings on insulating Quartz substrates is measured with the four point method to eleminate the effect of possible contact resistance at the contact points between Nb film and the pins of the measuring device. After measurement of the film resistance at room temperature the samples are cooled down in a helium bath to 10 K, what

is just above the transition temperature of Niobium (9.2 K). Then the low temperature resistance is measured and the RRR can be calculated.

To find the best sputtering configuration we use a stainless steel dummy cavity, where quartz samples can be connected. The Quartz substrates can be taken after each sputtering process and the properties of the films, produced under different conditions can be measured. The sample holders are distributed over the whole length of the cavity and are numbered from 1 to 5, according to figure 3-13

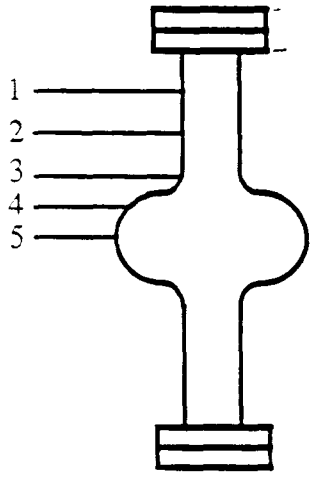

Fig. 3-13 *Distribution of the samples in the cavity*

The first experiments were made without temperature regulation. Under these circumstances the temperature of the cavity during the deposition grows within 10 minutes from room temperature up to 270° C. At this temperature the deposition was interrupted, because a further increase could result in an implosion due to copper softening. In order to reach a sufficient thickness 4 depositions of 10 minutes were made. The films showed RRR values of around 7 at the equator and up to 40 in the iris zone. Since the RRR value increases with grain size, the most promising way to reach better films is to deposit in only one step. So the grains can grow continuously and reach larger sizes. To prevent the heating to dangerous temperatures, a regulation system was developed, as described before. Herewith, prior to coating the equator was heated to 200° C and hold at this temperature during the hole processing time. The first films made in this way shows RRR values of 22 at the equator and 50

at the iris. The processing parameters were: Deposition power 2.5 kW, argon pressure $3.7*10^{-3}$ mbar, coils distance 9.5 cm. There is still room for further improvements looking for the optimum deposition parameters.

Power

In theory increasing the power, in order the deposition rate, the film quality should improve, because the number of trapped impurities during the deposition depends on the deposition time. If one deposit with higher rate the number of impurities decreases. Unfortunately in our experiments there was no significant improvement when we sputtered with higher power. We increase the power from 2.5 to 4 kW, but the films show only slightly better quality (RRR = 24 instead of 22). The reason for this behaviour can be that the impurities from residual gas was already rather low, so that no further improvement was possible.

Coils distance

Since the plasma-substrate interaction has a strongly influence of the film growing process and herewith of the film quality, one possibility to increase the RRR-values to find the optimum plasma parameters. In our case we can steer the plasma by varying the distance of the coils, varying the current, that passes the coils. in our experiments we found out, that the varying of the distance has indeed a remarkable influence of the plasma, whereas the coils current over an upper limit is not efficient. With changing the distance from 95 to 115 mm, the RRR value at the equator increase from 22 to 30, holding the other deposition parameters constant. with further increase of the coils distance, the film quality begins to decrease. The optimum current, that provide an satisfactory stability of the plasma confinement was found with 1.4 A.

4. Radiofrequency Tests

4.1 The RF measurement device

To measure the fundamental parameters like Q_0 and E_{acc} of a cavity a rf measurement system is constructed at INFN-LNL. In this short introduction the basic working principle should be explained. The main parts of the system are represented by the

-1.5GHz RF generator
- reflectometer
- movable input coupler
- pick-up antenna
- feedback loop

They are arranged as shown in Fig.4-1.

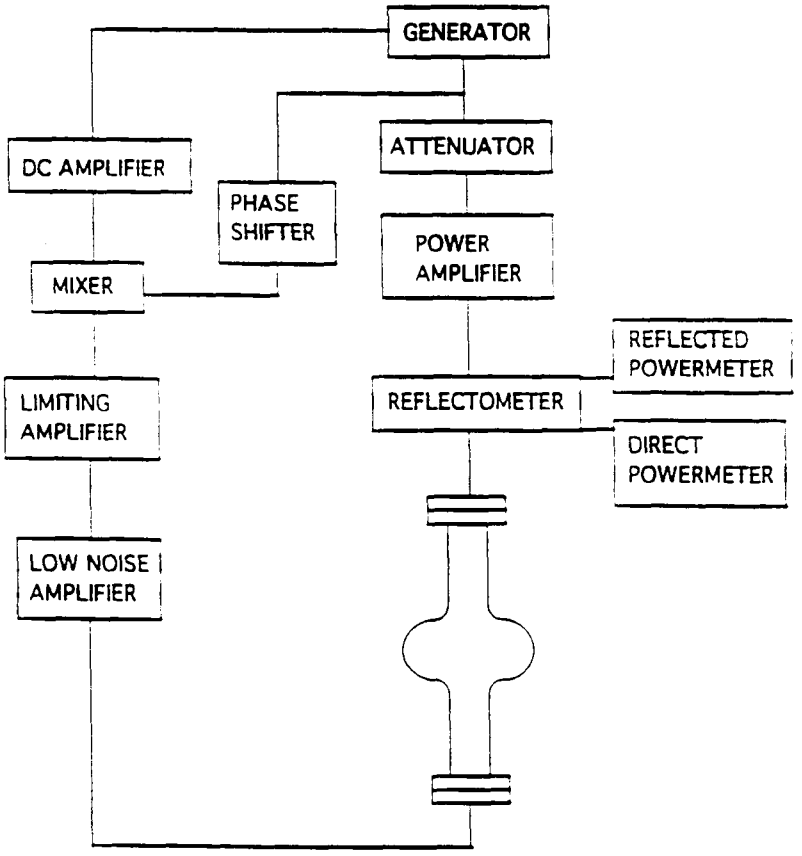

Fig. 4-1 Configuration of the radiofrequency system

The system is designed in such a way that all critical parts are computer controlled. The working principle is as follows: A generator produces the RF signal, the amplitude of the signal is regulated by the attenuator. Then it passes through the reflectometer, which measures the part of the signal that goes into the cavity and the one that is reflected. Through the moveable input coupler the signal enters the cavity. The pickup-antenna gets the response from the cavity, that then amplified and limited in the amplitude comes to one of the inputs of the mixer. To the other input the initial signal from generator passed through the phase shifter is applied as reference. The mixer is working as phase detector, having at the inputs two signals with the same frequency and amplitude, but different phases. From the mixer output the signal, proportional to the phase shift between the reference signal and the one passed through the cavity, goes to DC amplifier and then is used to correct the frequency of generator. All this structure represents the phase-lock loop, that is needed to have the system working at the resonant frequency of the cavity during the measurement. The precise adjustment of the phase-lock loop is done with phase shifter and moveable coupler to minimise the reflected signal and to maximise the cavity response. To find the cavity resonant frequency of 1.5GHz is rather difficult, because the bandwidth of a superconducting cavity is about 10 Hz. To measure the Qo-factor a rf power of about 1mW will put inside the cavity. Then the power supply will be switched off and the electromagnetic field inside the cavity begins to decay. From the decay time one can calculate the Qo factor according to the formula

$$W(t) = W_0 \cdot e^{-W_0 Q t} \qquad (4.1)$$

Knowing the geometrical constants and using the results of the decay time measurement one can find the coefficient between the pickup signal and accelerating field of the cavity. To measure the dependence of Qo versus E_{acc} the input power will be increased up to 10~30W. But sometimes the behaviour of the cavities can be unpredictable, due to that the main control panel is designed in a way to give complete manual control of the measurement. The automatic procedures can be activated manually and after fulfilling them the system returns to the manual mode. The

automatic procedures are the following: calibration, search for the resonant frequency, minimisation of the reflected power, measurement of the decay time, Q versus accelerating field measurement, conditioning.

4.2 Related cryogenics

For the rf test measurements the cavity had to be cooled up to 1.8 K by a cryostat. The cryostat is constructed and built at INFN-LNL, copying a design of CERN laboratories.
The main construction elements of the cryostat are:

- shielding of transfer line
- seperator
- precooling valve
- thermo exchange 1.8 K - 4.2 K
- expansion and level regulation valve

They are placed as shown in fig. 4-2

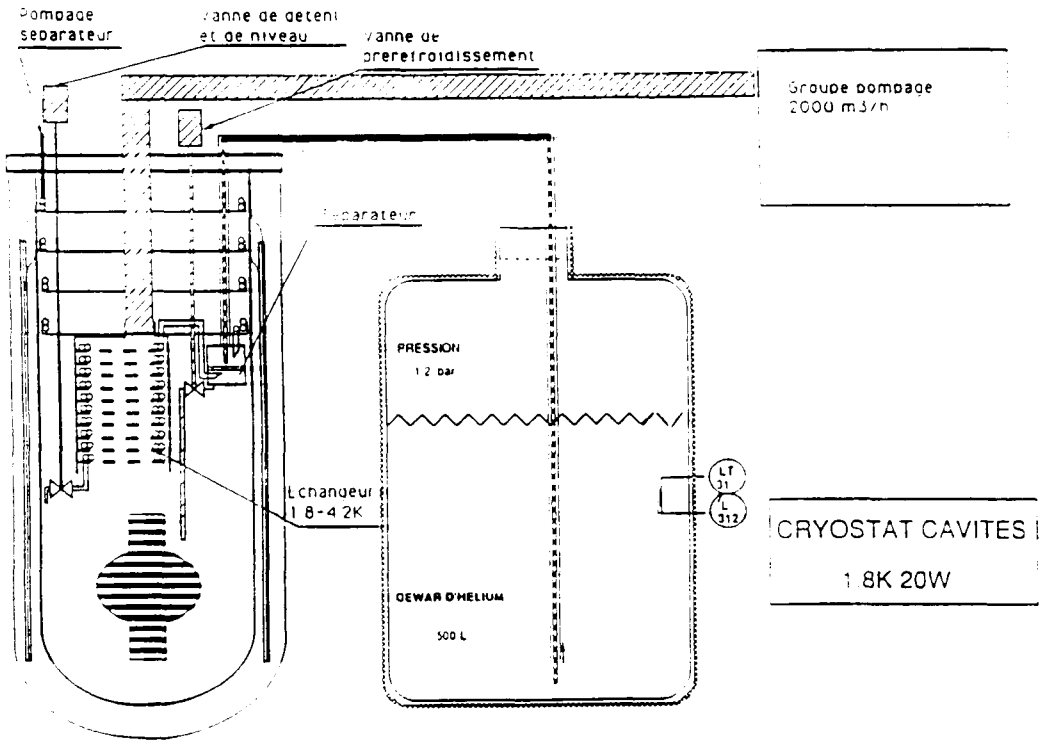

Fig. 4-2 Setup of the cryogenic system [43]

The operating modes of the cryostat are the following:

- Cooling to 4.2K and measuring test at this temperature
- Pumping one shot at 1.8 K without level regulation, with a dissipated power less than 1 W.
- Possibility to cool continuously from 4.2 K to 1.8 K with a relaxation valve to regulate the Helium level. The system is equipped with a pumping group of 2000 m^3/h to reach a maximum dissipated power of 20 W at 1.8 K.

The cryostat is alimented by a dewar of a volume of 500 l. The helium coming from the dewar through the transfer line goes to a cover that emerge into the seperator. After passing the transfer line the helium contain vapour, that is divided from the liquid by the seperator. These vapours are used to thermalize the screens of the cryostat and could be also used to cool quickly some certain zones of the cavity. The three thermo screens are cooled by the vapour, which is pumped by a membrane pump. The task of this pump is not only to suffer the screens with vapour, but also to keep the transfer line at a constant temperature of 4.2 K. The vapour flow is regulated by a valve, to reach a constant pumping speed of $1 m^3/h$ The liquid helium is filtered by the sinter bronze and leave the seperator by two tubes. One leads to the valve for precooling the cavity to 4.2 K and to fill the cryostat up to a certain level with helium. The other tube leads to the thermo exchange 1.8-4.2 K.

To reach temperatures less than 4.2 K one method is to pump the vapour over the liquid helium bath. So the atoms in the bath with higher velocity leave the bath and only slower atoms remain. That means that the temperature decreases. With a roots pump of 2000 m^3/h pumping speed it is possible to reach a temperature of 1.8 K, even when a power of 20 W is dissipated in the Helium bath. To have the possibility to work with varying values of dissipated power the rotation velocity of the pump can be regulated. Certainly the volume of the bath decrease, when it starts to evaporate due to the pumping. To provide a constant level an regulation valve is needed. The tasks of this valve is to provide a constant level of

Helium and to reduce the pressure of the entreating Helium from 1 bar to 16mbar, which is the pressure over the bath at 1.8 K. The valve is equipped with a needle, which has a double slope, to overcome the difference in viscosity between normal and superfluid Helium. At 16 mbar the relaxation of helium of 4.2 K leads to a evaporation of 50 %. To reduce this percentage to 20 % and so to increase the available power a heat exchange between pumped vapour and liquid helium is needed. With this thermo exchange the helium arrive with 2.2 K to the bath.
Due to the high price the roots pump with 2000 m^3/h pumping speed is replaced by a pump with lower speed. In first tests a temperature around 2 K is reached. Unfortunately it is not possible to dissipate any power at this temperature, what is needed to measure the Qo versus accelerating field.

4.3 MEASUREMENT OF THE FIRST SPUTTERED SPUN CAVITY.

A fully spun seamless cavity was used as a substrate for sputtering. This was the first time that a cavity in this way was produced. The advantages of a seamless forming are twofold: First of all it provides an internal surface without unevenness due to electron beam welding. Usually two half-cups are welded together. this leads to a rough surface in the equator-zone. Furthermore even microholes can appear in the copper material which can be opened during the electropolishing. The second advantage is the fact that this method is in opposite to common techniques like hydroforming appliable without annealing and much less expensive.

The general treatment of the substrate before deposition is as follows:

1. Electropolishing with a solution of phosphoric acid and n-butanol. By this process 100 µm of the copper are etched from the surface.
2 Chemical polishing which takes away additional 5 µm followed by a passivation to prevent further contaminations of the substrate

The deposition conditions were in a primary step attempted, as described in the preceding chapter. The particular parameters applied for the sputtering procedure are presented in this schedule:

- Voltage: 570 V
- Current: 5.3 A
- Temperature: 200°C
- Current of the external coils: 1.5 A
- Current of the internal coils: 1.5 A
- Coils gap: 115 mm
- Deposition time: 30 min.

This leads to a thickness at the equator of 2.5µm and5µm in the iris. After finishing this step the cavity is mounted into the cryostat. where it is cooled down to a temperature of 4.2 K and the measurements of the Q vs Eacc was carried out. The result is shown in fig 4-3

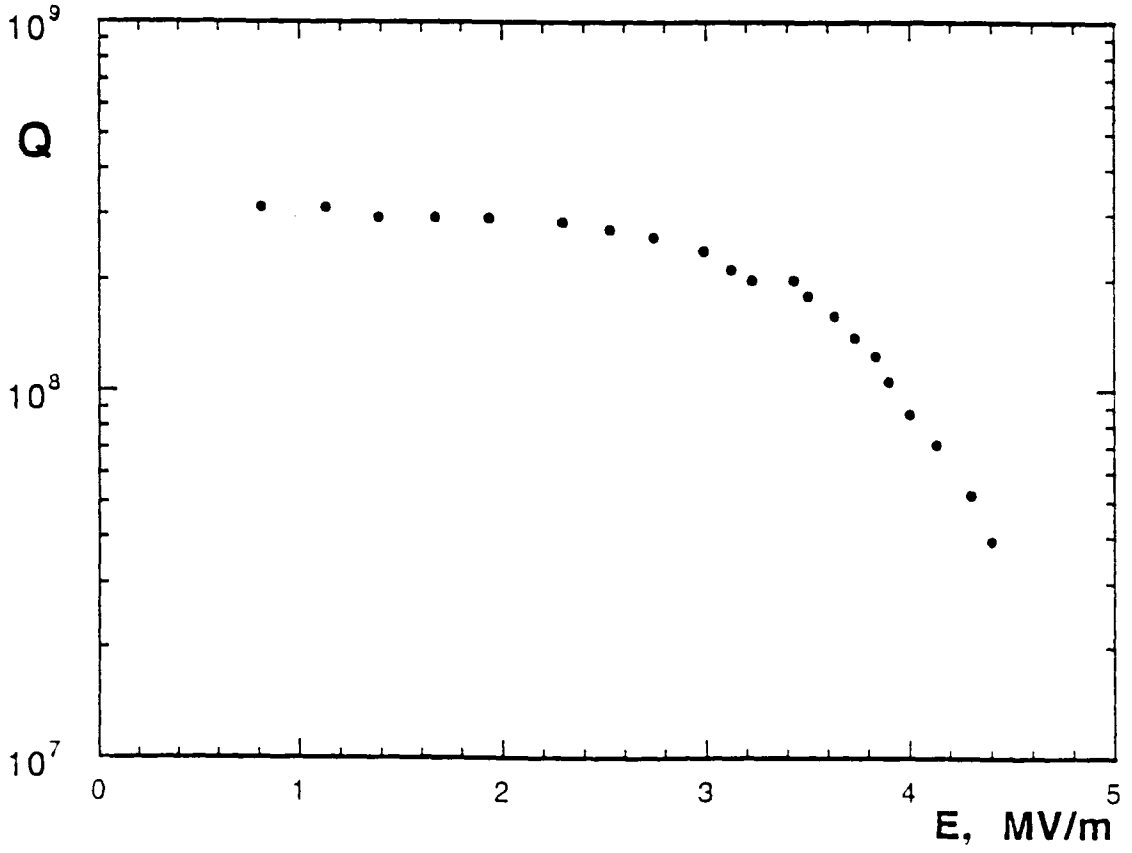

Fig 4-3 *Q versus Eacc*

From the figure one can see that Q does not exceed $3 \cdot 10^8$. The slope of the curve is up to 3 MV/m rather small and after passing this value it decreases stronger. With helium conditioning usually the Eacc of the cavity can be improved by a factor two. Helium conditioning is the applying of radiofrequency high power into the cavity which is filled helium gas at a pressure of 10^{-5} mbar. This leads to a surface bombardement with helium ions of high energy. which sweeps away chemisorptions and cryoabsorbed atoms from the cavity surface.

Unfortunately due to a destruction of a part of the system this processing could not be done. Probably higher values of Qo and Eacc could be reached.

5. Conclusions

The following informations can be extracted from our measurement:

- Even if the values of RRR that we obtained in the dummy cavity sputtering in the same conditions are rather high, the Q-factor at 4.2 K is lower than 4. 10^8. In our opinion this is due to imperfections of the substrate. Some ferrous contamination can be bared inside Copper on the side of the internal surface. Such foreigner inclusions are not removed by electropolishing and they cause microscopic holes in the film.
- We did not yet achieve high fields, however we do not see any slope for the Q-degradation versus accelerating field, that is the worst enemy for sputtered cavities.

Even if this was the first time that a cavity was formed by spinning from a copper disc and internally sputtered with niobium, the achieved results are not bad and we proved successfully, that this is the right way for future research. However, our results are only preliminar. Nevertheless we can state at least two concepts: a) the magnetron configuration has a high potential, especially from the point of view for the application to 1.3 Ghz ninecell cavities. b) there is no any principle argument against the spinning technique applied to the construction of Copper resonators for sputtering

Central aim for future research will be the optimising of the interface between copper substrate and niobium film.

Appendix

In order to find the best deposition parameters for sputtering the copper prototype we have performed several depositions in the stainless steel dummy cavity, equipped with Quartz samples. For each run we have compilled a coating schedule in which the main RRR and the thickness are reported.

\
Date: 06.12.94

SAMPLE #	1	2	3	4	5
RRR	11.6	9.68	6.85	6.11	39.9
t / μm	1	1.1	0.7	0.5	1.9

Deposition parameters:
Time: 2 depositions a 5 min
Power: 2.5 kW
Temperature: increasing during the deposition from 20°C to 300°C
Coils distance: 9.5 cm

Date: 13.12.94

SAMPLE #	1	2	3	4	5
RRR	6.27	14.5	5.29	5.41	33.7
t / μm	0.7	1.1	0.7	0.5	1.4

Deposition parameters:
Time: 2 depositions a 5 min
Power: 2.5 kW
Temperature: increasing during the deposition from 20°C to 320°C
Coils distance: 9.5 cm

Date: 12.01.95

SAMPLE #	1	2	3	4	5
RRR	*	9.34	6.67	6.03	45.3
t / µm	*	2.0	1.4	1.1	2.5

Deposition parameters:
Time: 4 depositions a 5 min
Power: 2.5 kW
Temperature: increasing during the deposition from 20°C to 310°C
Coils distance: 9.5 cm

Date: 31.01.95

SAMPLE #	1	2	3	4	5
RRR	13.8	23.0	9.56	11.0	50.5
t / µm	2.3	3.2	1.8	1.7	5.0

Deposition parameters:
Time: 5 depositions a 5 min
Power: 2.5 kW
Temperature: increasing during the deposition from 20°C to 270°C
Coils distance: 9.5 cm

Date: 21.02.95

SAMPLE #	1	2	3	4	5
RRR	35.0	*	22.5	23.6	50.0
t / µm	2.9	*	2.1	1.8	4.5

Deposition parameters:
Time: 25 min
Power: 2.5 kW
Temperature: 200°C
Coils distance: 9.5 cm

Date: 24.02.95

SAMPLE #	1	2	3	4	5
RRR	27.6	*	14.9	15.5	51.0
t / µm	2.3	*	1.5	1.7	3.6

Deposition parameters:
Time: 20 min; interuption by closed valve
Power: 2.5 kW
Temperature: 250°C
Coils distance: 9.5 cm

Date: 03.03.95

SAMPLE #	1	2	3	4	5
RRR	*	30.0	21.5	20.5	42.7
t / µm	*	2.8	1.6	1.8	4

Deposition parameters:
Time: 25 min
Power: 2.5 kW
Temperature: 250°C
Coils distance: 9.5 cm

Date: 07.03.95

SAMPLE #	1	2	3	4	5
RRR	36.1	35.5	31.3	23.5	51.5
t / µm	3.1	4.3	2.8	2.7	5.1

Deposition parameters:
Time: 40 min
Power: 2.5 kW
Temperature: 250°C
Coils distance: 9.5 cm

Date: 21.03.95
Plasma instabilities due to not symmetrical configuration of coils

SAMPLE #	1	2	3	4	5
RRR					
t / µm	4.0	4.4	2.3	1.8	5.4

Deposition parameters:
Time: 40 min
Power: 2.5 kW
Temperature: 250°C
Coils distance: 9.5 cm

Date: 27.03.95

SAMPLE #	1	2	3	4	5
RRR	34.5	43.5	23.5	26.9	53.5
t / µm	4.3	4.0	2.1	2.0	5.8

Deposition parameters:
Time: 25 min
Power: 4 kW
Temperature: 250°C
Coils distance: 9.5 cm

Date: 05.04.95

SAMPLE #	1	2	3	4	5
RRR	*	55.3	25.4	22.0	55
t / µm	*	2.3	1.3	1.5	2.7

Deposition parameters:
Time: 15 min
Power: 4 kW
Temperature: 250°C
Coils distance: 10.5 cm

Date: 10.04.95

SAMPLE #	1	2	3	4	5
RRR	*	45.0	33.4	34.7	60.0
t / µm	*	3.5	2.6	2.3	5.9

Deposition parameters:
Time: 28 min
Power: 3 kW
Temperature: 200°C
Coils distance: 10.5 cm

Date: 28.04.95

SAMPLE #	1	2	3	4	5
RRR	39.4	55.2	23.5	33.8	50.5
t / µm	4.5	4.8	2.7	2.5	5.2

Deposition parameters:
Time: 30 min
Power: 3 kW
Temperature: 200°C
Coils distance: 14 cm

Date: 03.05.95
Due to plasma instabilities during the deposition no RRR measuring

SAMPLE #	1	2	3	4	5
RRR					
t / µm	2.2	2.6	1.8	2.6	5.2

Deposition parameters:
Time: 28 min
Power: 3 kW
Temperature: 200°C
Coils distance: 16 cm

Date: 31.05.95

SAMPLE #	1	2	3	4	5
RRR	39.7	*	29.0	27.6	45.0
t / µm	2.9	3.5	2.5	2.3	4.8

Deposition parameters:
Time: 30 min
Power: 3 kW
Temperature: 200°C
Coils distance: 12 cm

Date: 16.06.95

SAMPLE #	1	2	3	4	5
RRR	39.3	46.1	27.0	31.7	70
t / µm	2.4	2.9	2.6	1.9	5.0

Deposition parameters:
Time: 30 min
Power: 3 kW
Temperature: 200°C
Coils distance: 12 cm

6. References

1 Tesla Collaboration, TESLA Test Facility Linac Design Report Version 1, March 95

2 Feynman, The Feynman lectures on Physics, vol. II, Addison-Wesley Publishing Company, Reading, 1964

3 H. Piel, in CERN Accelerator School: Superconductivity in Particle Accelerators, ed. S. Turner, p.149 ff., CERN 89-04, 1989

4 J. D. Jackson, Classical Electrodynamics, John Wiley & Sons, New York, 1962

5 H. Kammerlingh Onnes, Comm. Phys. Lab., Univ. Leyden. 1911

6 D. J. Quinn a. W.B. Ittner: J. Appl. Phys. 33, 748, (1962)

7 J. G. Bednorz, K.A. Mueller, Z. PHYS. B, 64 (1986) 189

8 Vladimir Z. Kresin and Stuart A. Wolf, Fundamentals of Superconductivity, Plenum Press, New York, 1990

9 W. Meissner and R. Ochsenfeld, Naturwiss., 21 (1933) 787

10 W. Buckel, Supraleitung, Grundlagen und Anwendungen, VCH Verlagsgesellschaft mbh, Weinheim, 1994

11 J. Bardeen, L.N. Cooper, J.R. Schrieffer, Phys. Rev., 108, (1957) 1175

12 H. Padamsee, CLNS 90-1004, Review Lecture presented at the 1989/1990 US Particle Accelerator School, Brookhaven National Lab., July 1989

13 V. Palmieri, R. Preciso, V.L. Ruzinow, S.Yu. Stark, I.I. Kulik, "Forming of seamlessaccelerating resonators of the reentrant type by the spinning technique", Submitted to Nuclear Insrtuments and methods in Physics research A342, 1994

14 G.Cavallari, C. Benvenuti, P.Bernard, E. Chiavieri, F. Genesio, E. Haebel, N. Hilleret, J. Tueckmantel, W. Weingarten, CERN-AT/93-10 (RF), presented at the IEEE PAC 93, Washington D.C.

15 C. Benvenuti in: Proc. of the V Workshop on RF Superconductivity, D .Proch, ed, DESY Report, M92-1 (DESY, Hamburg, 1992 p.184)

16 Ph. Bernard, D. Bloess, W. Hartung, C. Hauviller, W. Weingarten, P. Bosland, J. Martignac: Proc. of the V Workshop on RF Superconductivity, ed D. Proch, DESY-Report, M92-1 (DESY, Hamburg, 1992 p.487)

17 M. Okuda et. al.: Proc. of the V Workshop on RF Superconductivity,

18 J. Halbritter, J. Appl. Phys. 42, 82, (1971)

19 J. Halbritter, J. Less. common metals 139, 133 (1988)

20 P. Kneisel, O. Stolz, J. Halbritter, J. Appl. Phys., 45, 2296 (1974)

21 J. Halbritter, Phys. Lett. 49A, 397 (1974)

22 A.M.Portis, "Microwaves and Superconductivity: Process in the intergranular coupling ", Springer Series in Solid State Sciences, ed J. Bednorz and K.A. Mueller, Springer Verlag, Heidelberg (1989)

23 M. Peiniger et al. 3-th RF Superconductivity Workshop, Argonne, (Sept 1987)

24 S.V. Vonsovsky, Yu.A. Izyumov, E.Z. Kurmaev, Superconductivity of transition metals, Springer Verlag (1977)

25 A. Junod, J.L. Staudemann, J. Muller, P.. Spitzli: J. Low Temp. Phys. 5, 25 (1971)

26 Jean Muller, A-15-type superconductors, Rep.Prog.Phys., Vol.43, (1980)

27 Alloy Phase Diagrams, Volume 3, ASM International (1990)

28 P. Sspitzli: Phys. Kondens. Met. 42,355 (1975)

29 D.J. Waterstraat, R.M. Bardos, T.J. Rowland: J. Low Temp. Phys. 3, 509 (1970)

30 R. Fluekiger: Superconductor Materials Science, Plenum Press, NewYork(1981)

31 B.M. Klein, L.L. Boyer, D.A. Papaconstantopoulos: J.Phys. 678 Paris, 1978

32 Klabund, "Thin films from free atoms and particles", Academic Press, INC. (1979)

33 Rene A. Haefer, "Oberflaechen und Duennschicht-technik", WFT Springer Verlag, 1987

34 Wehner, G. K.: Anderson, G. S.: Handbook of thin film technology, New York, Mc Graw-Hill 1970

35 Fetz, H.; Oechsner, H.: Compt. Rend. VI CIPIG, Paris (1963) vol 2, p. 39

36 Almen, O.; Bruce, G.: Trans. 8th Nat. Vac. Symp. (1962) 245

37 Kaminsky, M.: Atomic and ionic impact phenomena on metal surfaces, Springer Verlag, Berlin (1965)

38 Thornton, J.A.; Penfold, A.S.: Thin film processes, New York, Academic Press 1978, p. 75

39 Chopra, K.L.: Thin Film phenomena, New York, McGraw-Hill 1969

40 Thornton, J.A.: J. Vac. Sci. Technol. 11 (1974) 666

41 Thornton, J.A.: Thin Solid Films 54 (1978) 23